

**PERIPHERAL NERVE REGENERATION BY SYNTHETIC  
PEPTIDE NANOFIBERS**

A THESIS SUBMITTED TO  
THE GRADUATE SCHOOL OF ENGINEERING AND SCIENCE  
OF BILKENT UNIVERSITY  
IN PARTIAL FULFILLMENT OF THE REQUIREMENTS FOR  
THE DEGREE OF  
MASTER OF SCIENCE  
IN  
MATERIALS SCIENCE AND NANOTECHNOLOGY

By

Mevhibe Geer

August, 2016

# **PERIPHERAL NERVE REGENERATION BY SYNTHETIC PEPTIDE NANOFIBERS**

By Mevhibe Geer

August, 2016

We certify that we have read this thesis and that in our opinion it is fully adequate, in scope and in quality, as a thesis for the degree of Master of Science.

---

Mustafa zgr Gler (Advisor)

---

Aye Begm Tekinay (Co-Advisor)

---

aęlar Elbken

---

Yusuf kr aęlar

Approved for the Graduate School of Engineering and Science:

---

Levent Onural

Director of the Graduate School

# **ABSTRACT**

## **PERIPHERAL NERVE REGENERATION BY SYNTHETIC PEPTIDE NANOFIBERS**

Mevhibe Geçer

M.S. in Materials Science and Nanotechnology

Advisor: Mustafa Özgür Güler

Co-Advisor: Ayşe Begüm Tekinay

August, 2016

The peripheral nervous system (PNS) has a complex structure that consists of high numbers of nerve cells and communication networks between the central nervous system and the body parts. Unlike the central nervous system, the PNS exhibits a considerable capacity for regeneration; however, peripheral nerve injuries can nevertheless cause lifelong disability. Various methods are currently available for the treatment of nerve injuries, but autologous nerve grafting is considered as ‘the gold standard’. Donor site morbidity, neuroma formation and failure of functional recovery are some limitations of this technique, especially when used for the repair of long nerve gaps. Polymeric nerve conduits are clinically available alternatives to nerve grafting, and function by guiding the axonal growth and isolating the regenerating axon from the inhibitory environment present in the post-injury neuroma. In this thesis, we used peptide amphiphile molecules (PAs) that can self-assemble into the nanofibers and mimic both the structure and function of healthy ECM of nerve cells for sciatic nerve regeneration. Two bioactive PAs, LN-PA (derived from laminin) and GAG-PA

(derived from glycosaminoglycan), were tested for their ability to induce neural regeneration in a rat sciatic nerve model. Hollow nerve conduits were filled with peptide nanofiber gels, and electrophysiology and histology results were compared with autologous graft treated groups. Our results show that bioactive peptide nanofibers are able to boost regeneration and functional motor and sensory recovery. Electromyography results demonstrated that better signal transmission was observed in peptide nanofiber treated groups compared with empty conduits and autograft treated groups. Histological assessments also confirmed that bioactive peptide nanofiber treated groups exhibited better axonal regeneration. These results suggest that these biologically active PA nanofiber gels may be used as a biomaterial for peripheral nerve regeneration in clinical practice.

***Keywords:*** *Extracellular matrix, peptide nanofibers, peripheral nerve regeneration, sciatic nerve, polymeric nerve conduit*

# ÖZET

## SENTETİK PEPTİT NANOFİBERLERLE PERİFERİK SİNİR

### REJENERASYONU

Mevhibe Geçer

Malzeme Bilimi ve Nanoteknoloji, Yüksek Lisans

Tez danışmanı: Mustafa Özgür Güler

Eş Danışman: Ayşe Begüm Tekinay

Ağustos, 2016

Periferik sinir sistemi çok sayıda sinir hücresi ve merkezi sinir sistemi ile vücudun diğer organları arasındaki iletişim ağını kapsayan oldukça kompleks bir yapıya sahiptir. Periferik sinir hasarları ömür boyu sürebilecek sakatlıklara neden olmasına rağmen, merkezi sinir sisteminin aksine, periferik sinir sisteminde rejenerasyon mümkündür. Günümüzde çeşitli tedavi yöntemleri uygulanmaktadır fakat otogreft yöntemi altın standart olarak bilinmektedir. Donör bölgede görülen morbidite, nöroma oluşumu ve fonksiyonel iyileşmedeki başarısızlıklar, uzun sinir boşluklarını tedavi etmek için otogreft yöntemi kullanıldığında meydana gelebilecek sorunlardan birkaçıdır. Alternatif olarak klinik uygulamalarda polimerik sinir tüpleri aksonların uzaması için bir yönlendirme ve inhibe edici ortamdan izole etme amacıyla kullanılmaktadır. Bu tezde, siyatik sinir rejenerasyonu için, kendiliğinden bir araya gelerek nanofiberler oluşturabilen ve hem fonksiyonel hem de yapısal olarak sağlıklı sinir hücrelerinin hücreler arası matrikslerini taklit edebilen peptit amfifil molekülleri kullanılmıştır. Bu peptit amfifillerden, LN-PA molekülünün biyoaktif sekansı laminin

proteininden ve GAG-PA molekülünün biyoaktif sekansı glikozaminoglikandan türetilmiştir ve rat siyatik sinir hasarı modelinde rejenerasyona olan etkisini belirleyebilmek için kullanılmıştır. İçleri boş olan sinir tüpleri bu peptit nanofiber jeller ile doldurulmuştur, elde edilen elektrofizyoloji ve histoloji sonuçları otogreft uygulanan gruplar ile karşılaştırılmıştır. Sonuçlarımıza göre kullanılan biyoaktif peptit nanofiberlerin sinir rejenerasyonunu, motor ve duyuşal fonksiyonların geri kazanımını desteklediđi gösterilmiştir. Elektromiyografi sonuçlarına göre sinyal iletimi peptit nanofiber uygulanan gruplarda, boş tüp ve otogreft uygulaması yapılan gruplara göre daha iyidir. Ayrıca histoloji sonuçları ile aksonal rejenerasyonun biyoaktif peptit gruplarında daha iyi olduđu desteklenmiştir. Biyolojik olarak aktif peptit amfifil nanofiber jeller, klinik uygulamalarda periferik sinir rejenerasyonu için bir biyomalzeme olarak kullanılabilir.

*Anahtar kelimeler: Hücreler arası ortam, peptit nanofiberler, periferik sinir rejenerasyonu, siyatik sinir, polimerik sinir tüpü*

## ACKNOWLEDGEMENTS

Firstly, I would like to thank my advisors Prof. Mustafa Özgür Güler and Prof. Ayşe Begüm Tekinay for giving this unique opportunity to win valuable experiences. I also would like to thank all NBT and BML members for their precious friendships, contributions and providing such nice environment.

I would like to thank Prof. Dr. Ümit Hıdır Ulaş, Assoc. Prof. Dr. Fatih Zor and Assist. Prof. Dr. Hakan Akgün for their supports and collaborations for *in vivo* experiments. I would like to thank Dr. Büşra Mammadov for her guidance and helpful discussions. Especially my dear friend Nuray Gündüz, I will never forget your companionship during my three years and I hope that it will take to the bitter end. I also would like to thank Mustafa Güler, Zeynep Erdoğan and Zeynep Ergül Ülger for their technical supports and assistances. I would like to thank Melike Sever for her collaboration during my master studies and always being helpful to me.

Especially I am thankful to Alper Devrim Özkan, Meryem Hatip, Aygül Zengin, Yasin Tümtaş, Seher Üstün Yaylacı, Ayşe Özdemir, Aref Khaliy, Hepi Hari Susapto, Elif Arslan, Berna Şentürk, Gülcihan Gülseren, Gülistan Tansık, Şehmus Tohumeken, Fatih Yergöz, Aslı Çelebioğlu, Yelda Ertaş and Zeynep Aytaç.

I would like to thank the Scientific and Technological Research Council of Turkey, TÜBİTAK BİDEB 2210-C fellowship.

The most intimate thank goes to my dear husband Muhammed Abdullah Geçer. I will never end my master thesis without him and junior Muhammed. I also would like to

thank all Yakut and Geer family members. They always support and make me feel special.

# CONTENTS

ABSTRACT .....	iii
ÖZET .....	v
ACKNOWLEDGEMENT .....	vii
CONTENTS .....	ix
LIST OF FIGURES .....	xi
LIST OF TABLES .....	xvi
CHAPTER 1 INTRODUCTION .....	1
1.1. PERIPHERAL NERVE INJURY AND REPAIR .....	2
1.1.1. The Gold Standard of Peripheral Nerve Injury: Autograft.....	7
1.1.2. Regeneration within Nerve Conduits .....	8
1.2. ECM MOLECULES AND THEIR FUNCTIONS IN PERIPHERAL NERVE REGENERATION.....	13
1.2.1. Neurotrophic Factors.....	16
1.3. INNOVATIVE DESIGN OF ECM MIMICING SCAFFOLDS.....	17
1.4. SELF-ASSEMBLED PEPTIDE NANOFIBERS AS SCAFFOLDS IN PERIPHERAL NERVE REGENERATION.....	21
CHAPTER 2 SCIATIC NERVE REGENERATION INDUCED BY GLYCOSAMINOGLYCAN AND LAMININ MIMETIC PEPTIDE NANOFIBER GELS .....	26
2.1. INTRODUCTION.....	27
2.2. MATERIALS AND METHODS .....	30
2.2.1. Materials .....	30
2.2.2. Synthesis and Purification of Peptide Amphiphile Molecules .....	31
2.2.3. Physical, Mechanical and Chemical Characterization of Self-assembled Nanofiber Network .....	33
2.2.3.1 Scanning Electron Microscopy (SEM).....	33
2.2.3.2. Oscillatory Rheology.....	33

2.2.4. Surgical Procedure .....	34
2.2.5. Electrophysiological Investigation .....	35
2.2.6. Histological Analysis .....	36
2.2.7. Ultrastructural Investigation .....	37
2.2.8. Statistical Analysis .....	38
2.3. RESULTS AND DISCUSSION .....	39
2.3.1. Synthesis and Purification of Peptide Amphiphile Molecules .....	39
2.3.2. Characterization of Peptide Amphiphile Nanofibers .....	46
2.3.3. Electrophysiological Assessment .....	50
2.3.4. Histological Assessment of Sciatic Nerve Tissues.....	53
2.3.5. Ultrastructural Assessment of Nerve Regeneration.....	62
CHAPTER 3 CONCLUSION AND FUTURE PERSPECTIVES.....	80
BIBLIOGRAPHY .....	84

## LIST OF FIGURES

**Figure 1.1.** Schematic view of the degeneration and the regeneration steps related with peripheral nerve injury. A: First few days after injury, the initial signs of axonal degeneration are present. B: Wallerian degeneration continues to progress, penetrating macrophages are recruited to remove cell debris. C: A large number of axonal sprouts pass through the injury site and reach the distal site of the axon with the assistance of Schwann cells in the bands of Bügner. D: Successful elongation and regeneration allows the restoration of signal transmission. E: Inappropriate regeneration and elongation of sprouts from the proximal stump to the distal stump of the injured axon results in neuroma formation. Adapted from Ref. [2] with permission..... **3**

**Figure 1.2.** An ideally designed nerve conduit should have a well-defined set of features to permit the outgrowth and regeneration of peripheral nerve cells. Copyright © 2006 Foundation for Cellular and Molecular Medicine/Blackwell Publishing Ltd. Reproduced from Ref. [44] with permission..... **9**

**Figure 1.3.** An illustration of the extracellular matrix, consisting of collagen fiber bridges that extend over cells through integrins located on the plasma membrane (A). Scanning electron micrograph of engineered self-assembled nanofiber scaffold (B) mimicking the native ECM. Reproduced with permission from Pearson Education, Inc., publishing as Benjamin Cummings. .... **20**

**Figure 1.4.** Chemical structure of IKVAV-PA molecule, showing four different regions (A). Graphical illustration of peptide amphiphile molecule and its self-assembly into a complex nanostructure (B). SEM image of peptide nanofiber scaffold demonstrates the similarity of the network structure of the natural ECM (C). TEM

image of IKVAV nanofibers (D). Copyright © 2001 American Association for the Advancement of Science. Reproduced with permission from Ref. [109]..... **23**

**Figure 2.1.** Images of electrophysiological assessment shows supramaximal stimulus (a) and the location of needle electrodes on solues muscles (a-b). ..... **35**

**Figure 2.2.** Chemical representations of peptide amphiphile molecules. Bioactive PA molecules; LN-PA (a) and GAG-PA (b). Positively charged PA molecule K-PA (c) and negatively charged molecule E-PA (d). Lauric acid tails are shown as black, beta sheet building blocks are red, charged units are blue and bioactive building blocks are shown as green. .... **41**

**Figure 2.3.** Liquid chromatography (A) and mass spectrometry (B) analysis of LN-PA ..... **42**

**Figure 2.4.** Liquid chromatography (A) and mass spectrometry (B) analysis of GAG-PA ..... **43**

**Figure 2.5.** Liquid chromatography (A) and mass spectrometry (B) analysis of E-PA. .... **44**

**Figure 2.6.** Liquid chromatography (A) and mass spectrometry (B) analysis of K-PA. .... **45**

**Figure 2.7.** Scanning electron microscopy images of nanofibrous scaffold PA gels surfaces. LN-PA/GAG-PA (**A, B**), K-PA/E-PA (**C, D**). Scale bars are 1  $\mu\text{m}$  (**A, C**) and 5  $\mu\text{m}$  (**B, D**) ..... **47**

**Figure 2.8.** Storage and loss modulus measurements of peptide amphiphile gels by oscillatory rheology. Rheology results showed that the mixture of peptide amphiphiles are soft materials suitable for neural tissue applications..... **49**

<b>Figure 2.9.</b> Functional evaluation of transected nerve by the measurement of amplitude.....	<b>51</b>
<b>Figure 2.10.</b> The results of evoked potential at 12 weeks after surgery.....	<b>52</b>
<b>Figure 2.11.</b> Hematoxylin & Eosin (H&E) staining of sciatic nerve tissue specimens: (p) proximal, (d) distal. Scale bars are 50 $\mu$ m. ....	<b>57</b>
<b>Figure 2.12.</b> Immunohistochemical staining of sciatic nerve tissue specimens with anti S-100 antibody: (p) proximal, (d) distal. Scale bars are 50 $\mu$ m. ....	<b>60</b>
<b>Figure 2.13.</b> Immunohistochemical staining of sciatic nerve tissue specimens with anti $\beta$ -III-Tubulin antibody: (p) proximal, (d) distal. Scale bars are 50 $\mu$ m. ....	<b>61</b>
<b>Figure 2.14.</b> Toluidine Blue-O stained semi-thin transverse sections of resin embedded tissues. Schwann cells are indicated with white arrows. LN-PA/GAG-PA (A-C), Healthy (D) groups. Scale bars are 100 $\mu$ m.. ....	<b>64</b>
<b>Figure 2.15.</b> Toluidine Blue-O stained semi-thin transverse sections of resin embedded tissues. K-PA/E-PA (A-C), Healthy (D) groups. Scale bars are 100 $\mu$ m. ....	<b>65</b>
<b>Figure 2.16.</b> Toluidine Blue-O stained semi-thin transverse sections of resin embedded tissues. Undefined morphological structures are indicated with black arrows. Sucrose (A-C), Healthy (D) groups. Scale bars are 100 $\mu$ m.....	<b>66</b>
<b>Figure 2.17.</b> Toluidine Blue-O stained semi-thin transverse sections of resin embedded tissues. Several stages of degeneration are indicated with white arrows. Autograft (A-C), Healthy (D) groups. Scale bars are 100 $\mu$ m.....	<b>67</b>
<b>Figure 2.18.</b> Quantification of the number myelinated axons/mm <sup>2</sup> from semi-thin sectioned sciatic nerve tissues stained with toluidine blue-O. Statistical analysis was performed with GraphPad Prism 5.01 applying One-way ANOVA.....	<b>68</b>

<b>Figure 2.19.</b> Transmission electron micrograph (TEM) of LN-PA/GAG-PA filled conduit treated group. Scale bars are 200 nm (A) and 500 nm (B-D). .....	<b>70</b>
<b>Figure 2.20.</b> Transmission electron micrograph (TEM) of K-PA/E-PA filled conduit treated group (A, B) and scanning transmission electron micrograph (STEM) of K-PA/E-PA filled conduit treated group (C, D). Scale bars are 200 nm (A), 500 nm (B-D). .....	<b>71</b>
<b>Figure 2.21.</b> Transmission electron micrograph (TEM) of sucrose filled conduit treated group (A, B) and scanning transmission electron micrograph (STEM) of sucrose filled conduit treated group (C, D). Scale bars are 200 nm (A), 500 nm (B, C) and 2 $\mu$ m (D). .....	<b>72</b>
<b>Figure 2.22.</b> Transmission electron micrograph (TEM) of autograft treated group (A, B) and scanning transmission electron micrograph (STEM) of autograft treated group (C, D). Scale bars are 200 nm (A, B), 500 nm (D) and 2 $\mu$ m (C). .....	<b>73</b>
<b>Figure 2.23.</b> Transmission electron micrograph (TEM) of healthy group (A-C) and scanning transmission electron micrograph (STEM) of healthy group (D). Scale bars are 500 nm (A-C) and 2 $\mu$ m (D). .....	<b>74</b>
<b>Figure 2.24.</b> Quantification axonal diameter of myelinated fibers on ultrathin transverse sections. Statistical analysis was performed with GraphPad Prism 5.01 applying One-way ANOVA ( $p < 0.05$ (*), $p < 0.01$ (**), $p < 0.001$ (***)) .....	<b>76</b>
<b>Figure 2.25.</b> Myelination thickness quantification of ultrathin transverse sections. Statistical analysis was performed with GraphPad Prism 5.01 applying One-way ANOVA ( $p < 0.001$ (***)). .....	<b>77</b>
<b>Figure 2.26.</b> Representative diagram indicating the critical nerve tissue fiber parameters. ....	<b>78</b>

**Figure 2.27.** G ratio quantification of ultrathin transverse sections. Statistical analysis was performed with GraphPad Prism 5.01 applying One-way ANOVA ( $p < 0.05$  (\*),  $p < 0.01$  (\*\*),  $p < 0.001$  (\*\*\*)). ..... **79**

## LIST OF TABLES

<b>Table 1.1</b> FDA-approved nerve guidance conduits with the name of company, degradation time, material and max gap length. Reproduced with permission from Ref. [65]. .....	<b>12</b>
<b>Table 2.1.</b> Sequence, molecular weight and net charge at pH 7 of peptide amphiphile molecules.....	<b>40</b>

**CHAPTER 1**  
**INTRODUCTION**

## **1.1. PERIPHERAL NERVE INJURY AND REPAIR**

The peripheral nervous system (PNS) contains the primary, sensory, motor, and autonomic neurons that are outside of the central nervous system (CNS), Schwann cells and ganglionic satellite cells. The brain is the principal organ that determines how an organism reacts to its external environment; however, this critical function relies strongly on the signals relayed by the peripheral nervous system. Peripheral neurons are composed of a cell body and an axon that can reach lengths in excess of one meter. Axons consist of short segments wrapped by an insulating sheath, called the myelin sheath, which is produced by Schwann cells and plays an important role during the nerve regeneration process. Axons are located in fascicles and surrounded by a perineurial sheath, while bundles of perineurial sheaths are in turn protected by an epineurial layer to form a complete peripheral nerve. Sensory neurons, which are responsible for carrying signals to the CNS, and motor neurons, which carry the messages from the CNS to internal organs, are the principal types of peripheral neurons.

Signal transmission throughout motor and sensory neurons enables the connection between the central nervous system and peripheral target organs. Peripheral nerve injuries (PNIs) disrupt this connection and are typically caused by physical trauma, such as vehicle accidents, falls and fractures. PNIs occur in every 1/40 trauma patients [1] and generally cause lifelong loss in nerve functions, potentially impairing the function of the target organ innervated by the injured neurons.

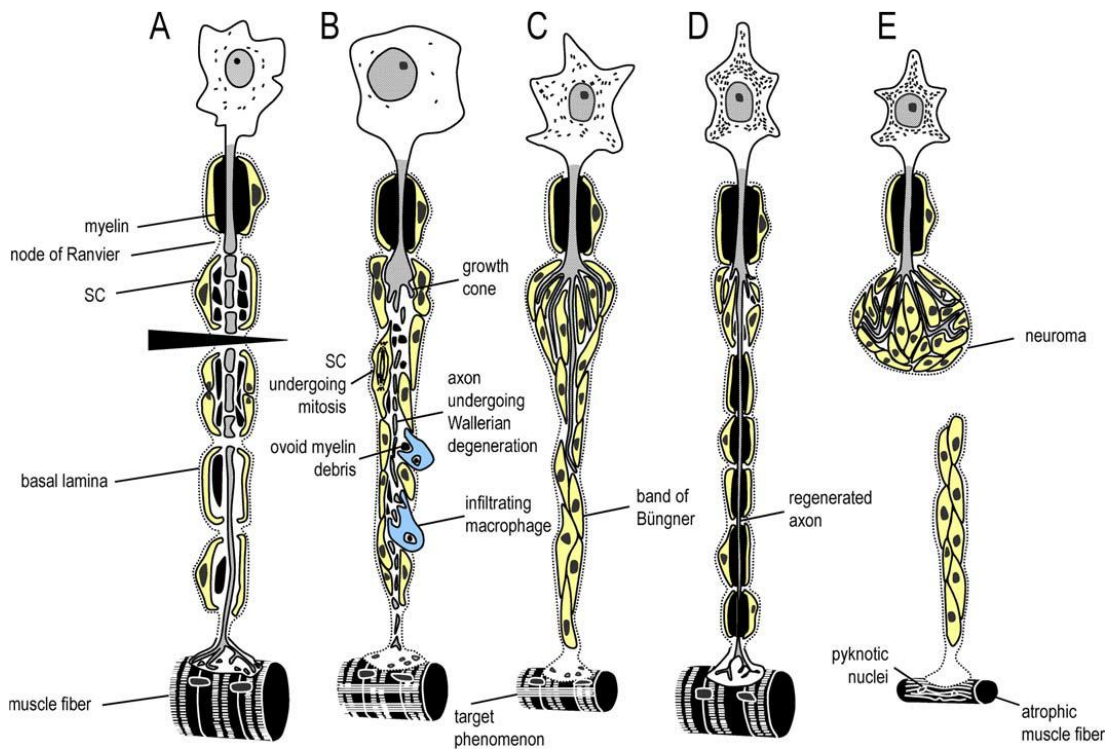


**Figure 1.1.** Schematic view of the degeneration and the regeneration steps associated with peripheral nerve injury. A: First few days after injury, the initial signs of axonal degeneration are present. B: Wallerian degeneration continues to progress, penetrating macrophages are recruited to remove cell debris. C: A large number of axonal sprouts pass through the injury site and reach the distal site of the axon with the assistance of Schwann cells in the bands of Büngner. D: Successful elongation and regeneration allows the restoration of signal transmission. E: Inappropriate regeneration and elongation of sprouts from the proximal stump to the distal stump of the injured axon results in neuroma formation. Adapted from Ref. [2] with permission.

Furthermore, PNI interferes with the quality-of-life and socio-economic circumstances of patients [3, 4]. According to a survey published in 2006, more than 100,000 patients undergo surgery in the USA and Europe each year for the treatment of nerve injuries [5].

Peripheral nerve injuries generally result in either good regeneration or painful neuroma formations that may result in severe muscle fiber atrophy. According to Sunderland [6], first and second degree peripheral nerve injuries (neurapraxia and axonotmesis) can be treated. The functional restoration is complete and morphological and physical damage is fully recoverable. Contrary to these milder conditions, the treatment of more severe injuries (*i.e.* those in which the endoneurial layer of the peripheral nerve is damaged, the nerve environment is ischemic, the axons undergo swelling and the myelin sheath cannot reverse its original morphology and function) are outside the scope of current medical treatments. In these injuries, reinnervation does not occur and impulse conduction is permanently interrupted.

Total functional recovery following nerve injury involves a complex series of degenerative and regenerative events (Figure 1.1). Before regeneration, the site of injury first experiences the local fragmentation of myelin sheaths, which directly stimulates the regeneration process (Figure 1.1A). In the first 6 hours following injury, nerve cell nuclei migrate to the edge of cells while Nissl granules and endoplasmic reticuli disassemble and disperse. This process is also known as chromatolysis and is necessary for the isolation of the neurons from the inhibitory environment prior to the recovery phase. However, cell survival cannot be ensured in severe nerve injuries; for instance, the frequency of apoptosis-related cell death in dorsal root ganglion (DRG)

neurons is between 20 to 50% under such cases [7]. In general, the steps of neuronal cell death are not understood in depth, but it is accepted that the microenvironment of the injury area is crucial for cell survival. For instance, many studies have showed that the isolated central neurons have the ability to regenerate when cultured in a PNS milieu, while isolated peripheral nerves do not regenerate in a CNS microenvironment [8, 9]. This regenerative difference between the PNS and the CNS microenvironments has been studied in detail and found to depend on the inductive roles of Schwann cells, ECM molecules and neurotrophic factors in the peripheral nerve milieu. In addition, growth factors such as fibroblast growth factor (FGF), nerve growth factor (NGF), brain-derived neurotrophic factor (BDNF) and other molecules enhance cell survival in the peripheral nervous system [10-12].

Morphologically, visible structural changes occur in the neuronal cell body while chromatolytic changes occur at the proximal injury site, where neuronal nuclei protrude from the cell bodies and the native nucleoproteins reassemble into Nissl granules (Figure 1.1B). During the chromatolytic process, numerous cellular activities are changed to induce RNA synthesis and reduce neurotransmitter production. Thus, neurons at the injury site are ready to produce the vast amount of proteins and lipids that are required for axonal outgrowth during the regeneration process. Fully functional recovery may take weeks to months and is reported to involve the reorganization and reconstitution of physical, morphological and functional connections at the injury site [13]. In peripheral nerve injuries [14], Schwann cells have a crucial role regarding the removal of axonal and myelin debris, the presence of which prevents axonal outgrowth in the distal nerve stump and interferes with the

secretion of ECM molecules and trophic factors [14], including laminins [15], the inflammatory cytokine IL-6 [16, 17], NGF [18-22] and FGF-2. Especially in the distal nerve region, Schwann cells and macrophages take part in removing tissue and cell debris and this process triggers cellular and functional changes related with Wallerian degeneration [23] (Figure 1.1A and 1B). Schwann cells proliferate and organize as columns, called bands of Büngner (Figure 1.1C). These bands are used as guides for the sprouting of axons across the basal laminae of Schwann cells, and serve as an early marker of neural regeneration [24, 25]. At the regenerating distal nerve site, interactions between mature Schwann cells and axons facilitate the remyelination process and create small internodes (Figure 1.1C). However, connective tissue scarring and impaired regeneration of seriously injured axons may cause abnormalities in the elongation process (Figure 1.1E). These types of PNI lead the formation of a neuroma in the proximal segment. Such abnormal formations have been accepted as an underlying reason of spontaneous neuropathic pain syndrome [26]. This ineffective regeneration causes an incomplete reinnervation, altering the alignment of Schwann cells in the distal nerve stump and inducing the production and deposition of endoneurial collagens. This denervation process negatively affects the function of the target end organ, and must generally be corrected through surgical intervention. There are various methods for the microsurgery repair of degraded PNI environments, including autograft/allograft transplantation, direct repair and hollow nerve conduits (NGC). Small nerve gaps can regenerate by themselves; however, transection gaps of over 5 mm in length are best repaired surgically by connecting the ends of nerve using sutures. This method is known as direct nerve repair [27-30].

### **1.1.1. The Gold Standard of Peripheral Nerve Injury: Autograft**

The autograft technique has served as a ‘gold standard’ for the treatment of peripheral nerve injuries for the last 50 years [28, 30]. Simple nerve grafting methods were initially described in the late 19<sup>th</sup> century, but autografting was only perfected decades later by Millesi, who optimized the technique and demonstrated its effectiveness over epineural suturing. Nerve grafts are preferably derived from less essential nerves, such as sural or cutaneous nerves, of the patient's own body [31]. Nevertheless, the operation has a rate of success under 50% [32, 33] and is associated with numerous limitations, such as donor site morbidity, formation of neuromas, possible loss of sensation and function, insufficient graft length, the necessity of secondary surgeries, mismatch of donor nerve owing to morphological differences, high cost to healthcare providers and the extension of the recovery time [33-37].

Autograft technique can be used for PNI treatment when the critical length of nerve gap is shorter than 5 cm, and beyond this length, allograft is an inevitable treatment [38]. However, this technique necessitates the use of immunosuppressives up to 2 years after surgery, and patients are prone to the threats coming from microenvironment which eventually results in tumor formation [39]. Consequently, these unfavorable consequences of autograft and allograft techniques are reasons to focus of efforts on alternative engineering strategies or devices for PNI repair. The use of nerve guidance conduits (NGCs) is the primary artificial tissue engineering technique.

### **1.1.2. Regeneration within Nerve Conduits**

Biochemically engineered nerve conduits have been found to be effective alternatives to autografting for the repair of damaged nerves. Hollow nerve conduits were first used for bridging a 30 mm nerve gap in a dog, using a bone conduit [40]. These hollow tubes present numerous advantages for PNI treatment, including isolation from the scar tissue, decreased formation of neuromas and scars and the aggregation of huge amounts of trophic factors, which allows these materials to provide an axon-guiding channel that connects the distal and proximal injury sites [7]. However, it should be noted that these NGCs are incapable of facilitating nerve repair over gap distances of 40 mm [41]. Nevertheless, the use of NGCs creates a well-defined microenvironment to modulate the neuronal repair process, allowing functional recovery of PNIs in clinical settings [42, 43].

An ideal nerve conduit should exhibit certain parameters to optimally facilitate the regeneration and reassociation of both elongated nerve fibers and components of the peripheral nerve system (Figure 1.2) [44]. These nerve conduits should permit the transition of neurotrophic factors released by Schwann cells and macrophages [45]. In addition, biocompatibility is a critical feature for any material intended for biological applications, and potential nerve conduits should therefore exert minimal toxicity and immunogenicity in living systems. Biodegradability is another desired feature, as the gradual removal of the scaffold material enhances the completion of the recovery process. Furthermore, a sufficient level of porosity should be maintained in the conduit environment to ensure the adequate distribution and diffusion of both endogenous and exogenous factors [46].

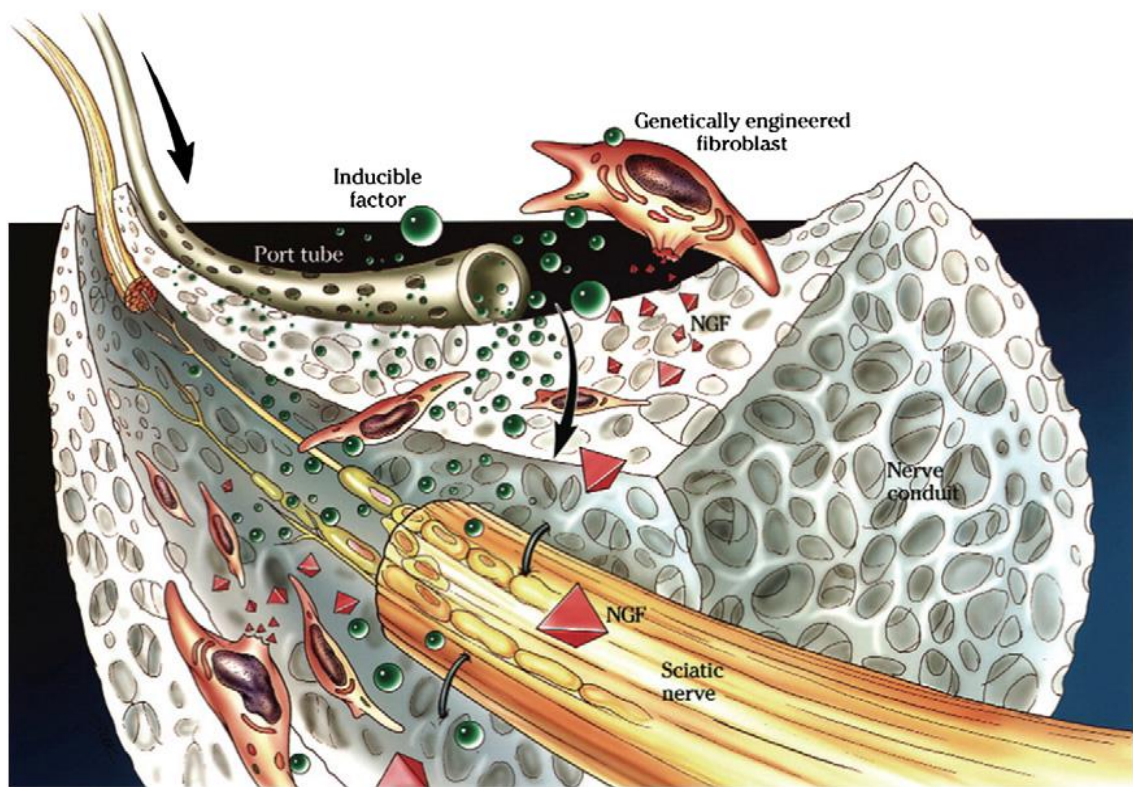


**Figure 1.2** An ideally designed nerve conduit should have a well-defined set of features to permit for the outgrowth and regeneration of peripheral nerve cells. Copyright © 2006 Foundation for Cellular and Molecular Medicine/Blackwell Publishing Ltd. Reproduced from Ref. [44] with permission.

The materials of nerve conduits are generally classified as synthetic [47] or natural [48]. Polyphosphoesters, aliphatic polyesters, hydrogel-based materials, polyurethanes and piezoelectric polymers are synthetic materials, while polysaccharides such as chitosan, collagen and decellularized scaffolds are animal derived natural materials. Polylactic acid (PLA), polyglycolic acid (PGA) [49, 50], polycaprolactone (PCL) [51-53], poly(lactide-caprolactone) (PLCL), poly(lactic-co-glycolic acid) (PLGA) [37, 54, 55], poly(3-hydroxybutyrate) (PHB), and various combinations of the PGA and PLCL

are some examples for aliphatic polyesters, which constitute one of the sub-classes of polymers. These polymers can be manufactured as fibers by electrospinning technique [56]. Collagen [57], laminin [58], chitosan [59] and other naturally derived polymers can also be used for the fabrication of nerve conduits.

It is well-established that peripheral nerve regeneration can be enhanced by using NGCs modified with biological and chemical moieties, soluble factors and natural or synthetic materials. As one example, a polysulfone NGC filled with laminin and NGF-loaded microtubules in a hydrogel matrix was found to enhance the regeneration of transected rat sciatic nerves with nerve gaps of 20 mm in length [60]. Biofunctionalization of hollow NGCs with growth factors or filling them with cells or stem cells are other strategies for bridging nerve gaps between injured nerve fibers [61]. These strategies can enhance axonal regrowth into the conduit and can also be used for the treatment of spinal cord injury [62].

The use of stem cells is another potential method for the enhancement of PNI repair. Stem cells are frequently delivered following their embedding in natural or synthetic platforms such as hydrogels or collagens that can be filled into NGCs. Chitosan NGCs filled with neural progenitor cells have been demonstrated to promote regeneration after spinal cord injury, and this conduit could also be functionalized with laminin to enhance neural adhesion and cell survival [63].

The US Food and Drug Administration (FDA) is a federal agency that is responsible for protecting public health in accordance with legal regulations. Many nerve guidance conduits and wraps have been approved by the FDA for use in the treatment of peripheral nerve injuries. FDA evaluates clinical products and devices with respect to

their safety, reliability and efficacy, and regards the use of nerve conduits as an effective means of enhancing peripheral nerve regeneration.

*Neurolac*<sup>®</sup> is one of the FDA-approved NGCs. Manufactured by Polyganics company, it is up to 3 cm in length and 1.5-10 mm in diameter (Table 1.1). This NGC is a synthetic, transparent and biodegradable scaffold that is produced from poly(DL-lactide- $\epsilon$ -caprolactone); it is hydrolysed within the body within 2 to 3 years. The use of *Neurolac*<sup>®</sup> is recommended for up to 2 cm gaps in PNIs. The advantages of *Neurolac*<sup>®</sup> include the reduction of neuroma formation [64].

**Table 1.1** FDA-approved nerve guidance conduits with the name of company, degradation time, material and max gap length.

Reproduced with permission from Ref. [65].

<b>Product Name</b>	<b>Material</b>	<b>Degradation Time</b>	<b>Company</b>	<b>Max Gap Length</b>
Neurolac	Poly(DL-lactic-co-1-caprolactone) (PLCL)	2-3 years	Polyganics Inc., The Netherlands	3 cm
Neurogen	Collagen type I	4 years	Integra Neurosciences, Plainsboru, NJ, USA	3 cm
Neuromend	Collagen type I	4-8 months	Collagen Matrix, Inc., Franklin Lakes, NJ, USA	2.5 cm
NeuraWrap	Collagen type I	4 years	Integra Neurosciences, Plainsboru, NJ, USA	4 cm
Neuromatrix/Neuroflex	Collagen type I	4-8 months	Collagen Matrix, Inc., Franklin Lakes, NJ, USA	2.5 cm
Neurotube	Woven polyglycolic acid (PGA)	6-12 months	Synovis Micro Companies Alliance, Birmingham, AL, USA	3 cm
Salubridge/Hydrosheath or Salutunnel	Salubria—polyvinyl alcohol (PVA) hydrogel	Non-biodegradable	Salumedica LLC, Atlanta, GA, USA	6.35 cm
Surgisis Nerve Cuff/ Axoguard	Porcine small intestinal submucosa (SIS) matrix	Not reported	Cook Biotech Products, West Lafayette, IN, USA	4 cm
AxonScaff/ Cellscaff or StemScaff	Polyhydroxybuturate (PHB)	Not reported	Axongen, Umea°, Sweden	Not reported

## **1.2. ECM MOLECULES AND THEIR FUNCTIONS IN PERIPHERAL NERVE REGENERATION**

Extracellular matrix (ECM) is a collection of a unique set of collagens, non-collagenous glycoproteins and proteoglycans that are produced by cells. The precise composition of the ECM is under strict regulatory control, and the expression levels of its constituent molecules are restricted to particular time periods both during development and in adulthood. The primary role of ECM molecules in the nervous system is the regulation of cell migration, survival, differentiation and axonal elongation in addition to structural support [66].

After PNI, the distal stump of the injury site begins to experience Wallerian degeneration, which involves the removal of cell debris and recruitment of macrophages to the site of injury, while the proximal nerve site initiates the regeneration process. However, the signals that trigger the regeneration of the proximal site have not been fully investigated [67]. PNI triggers both the endogenous and exogenous growth capacity of damaged neurons, which may induce the regeneration of the PNS [68]. Extracellular matrix proteins, neurotrophic factors and cell adhesion molecules all promote the successful axonal regeneration by activating the endogenous growth capability of the neural cell body.

This growth capacity is well-studied in a group of primary sensory neurons, the dorsal root ganglion cells (DRG). Myelin-associated glycoprotein (MAG) is able to inhibit DRG neurite outgrowth *in vitro*, but lesions in peripheral axons enhance the endogenous outgrowth capacity to cancel the inhibitory effects of MAG [69, 70].

Dibutyryl-cAMP, an analog of intracellular cyclic adenosinemonophosphate (cAMP), can also enhance axon growth capacity of the DRG after injury [69-71]. The activation of protein kinase A (PKA) by cAMP can cause the axonal elongation of sensory neurons cultured on MAG [69, 70]. In addition, PKA and cAMP can positively regulate the expression level of Arginase I, which is an enzyme related with polyamine synthesis after PNI. Therefore, the upregulation of Arginase I can abolish the inhibitory effect of MAG or myelin [72]. cAMP response element binding protein (CREB) expression is regulated transcriptionally by cAMP, which can reduce the inhibitory effect of MAG or myelin and result in the upregulation of neurite outgrowth and axonal regeneration *in vivo* [73]. c-Jun is another transcriptionally downregulated gene in PNI, and the knockout of c-Jun promotes neural regeneration after injury [74].

Laminin, an ECM glycoprotein, has a crucial role in axonal regeneration and is required for proper myelination by Schwann cells [75]. Laminin 8 ( $\alpha4\beta1\gamma1$ ) and laminin 2 ( $\alpha2\beta1\gamma1$ ) are two of the 15 accepted isoforms that are expressed largely in the endoneurial layer of PNS [15]. Synthesis of laminin is upregulated by Schwann cells at the injury site after PNI and this upregulation promotes regeneration [21, 76]. Consequently, laminin has an indispensable effect for neural regeneration. *In vitro* inhibition of neurite growth was shown by an anti- $\alpha2$  laminin chain blocker after sciatic nerve injury [77]. The  $\alpha$  chain of laminin, which contains the RGD and IKVAV sequences, has also been shown to promote neurite outgrowth in the PC-12 cell line [78] while antibodies against the IKVAV site disable the function of laminin by binding to its signaling sequences. Laminin interacts with cells through both integrins and  $\alpha$ -dystroglycans [79, 80] and its interaction with integrins is principally mediated by the two integrins  $\alpha1\beta1$  and  $\alpha3\beta1$ , in PC-12 cells [81]. ]. Laminin has an important

effect on Schwann cell behavior, including myelin production and ensheathment. Abrupt changes in laminin levels may therefore result in improper Schwann cell differentiation and hypomyelination [82].

Proteoglycans are strongly glycosylated proteins that constitute the majority of ECM components and receptors, and are found commonly in the basal lamina. These proteins have an important role for neuronal and axonal guidance. They are categorized into two major groups: heparan sulfate proteoglycans (HSPGs) and chondroitin sulfate proteoglycans (CSPGs). Cell surface proteoglycans bind to the ECM molecules and they are implicated as receptors for growth factors [83]. For example, FGF binds to both the core protein and glycosaminoglycan (GAG) moieties of heparan sulfate (HS) proteoglycans [84]. As a result of this interaction, proteolysis of FGF is blocked by proteoglycans and the ECM functions as a reservoir for FGF [85]. In addition to this interaction between FGF and HS, many other growth factors have been suggested to serve as mitogens for Schwann cells, triggering cellular proliferation by binding to HS [86]. HS chains present on different types of proteoglycans can interact with various growth factors, such as bFGF, aFGF, G-CSF, INF-1, and Il-3 [87].

Schwann cells promote the regeneration in the PNS by three ways: increasing the synthesis of cell adhesion molecules (CAMs) such as N-cadherin, L2/HNK-1 and NCAM; regulating the basement proteins such as laminin, fibronectin, HSPGs and tenascin; and releasing neurotrophic factors such as NGF, FGF-2, IGF, CNTF, GDNF, and BDNF. As a result, laminin plays a significant role in both the formation of neurite outgrowth and the proliferation and survival of Schwann cells.

### 1.2.1. Neurotrophic Factors

Neurotrophic factors and neurite growth inducing factors are fundamental for neural cell survival, axonal outgrowth and the regulation of Schwann cell behavior after PNI. Injury induced neuronal death will decrease the potency for axonal growth. The axonal outgrowth-promoting effect of neurotrophic factors and neurite outgrowth promoting factors, including NGF, neurotrophin 3 (NT-3), and brain-derived neurotrophic factor (BDNF), were shown by various *in vivo* studies and resulted in a comprehensive understanding of the signaling pathways involved [88]. The inductive effect of NGF on axonal growth was shown by both *in vivo* and *in vitro* studies [89]. Briefly, the NGF signaling pathway upregulates the activation of phosphatidylinositide 3-kinases (PI3K), while PI3K inhibits glycogen synthase kinase 3 (GSK-3 $\beta$ ) to promote axonal regeneration by regulating cytoskeleton proteins [88].

NGF exhibits an inducer effect on neurite outgrowth of DRGs by modulating the activity of laminin, but neither laminin nor NGF cannot induce sufficient axonal growth in PNS by themselves [90, 91]. Tyrosine kinase receptor B (trkB) and trkC are used for inducing the biological activities of BDNF, NT-3, and NT-4/5 [92, 93]. FGF-2 is also upregulated after PNI and the regulation of Schwann cell proliferation and differentiation is stimulated by FGF-2 [94]. The binding of neurotrophin factors to their receptors triggers the phosphorylation of tyrosine residues, resulting in cell proliferation and differentiation, while FGF-2 inhibits the expression of myelin gene and myelin zero protein [95]. Therefore, after sciatic nerve injury, FGF-2 boosts the number of axons while reducing the myelin sheath thickness. Ciliary neurotrophic factor (CNTF) is a survival factor enhancing synthesis of neurotransmitters and

promoting neural outgrowth after injury in the peripheral nervous system [96]. Although it has not so far been demonstrated to be effective in promoting nerve repair [97], it is plausible that this factor shows regenerative and functional impact in tandem with other neurotrophic factors [98].

TGF- $\beta$  helps the Schwann cells to stay in their proliferative state by inhibiting myelin production through development. Furthermore, after nerve injury, the release of TGF- $\beta$  is increased in the distal nerve stump by macrophages and Schwann cells, and the induced release of TGF- $\beta$  modulates Schwann cell behavior during axonal outgrowth [99, 100]. The binding of neurotrophic factors to their receptors triggers the phosphorylation of tyrosine residues, resulting in the proliferation and differentiation of Schwann cells and neurons.

### **1.3. INNOVATIVE NANODESIGN OF ECM MIMICING SCAFFOLDS**

Tissue engineering and regenerative medicine provide new strategies for the fabrication of biological scaffolds. However, the effective repair of damaged tissues and organs necessitates the development of top-down and the bottom-up processing methods that seamlessly integrate design principles associated with nanotechnology, material science and tissue engineering [101]. The applicability of new strategies often depends on two important factors, which are: (i) the biocompatibility of newly designed scaffolds, which should above all not be harmful to the body, (ii) their suitability for the differentiation of cells, and especially stem cells and primary cell

lines. Overall, when developing new strategies for the regeneration of damaged tissues or organs, the ideal material is a scaffold that can mimic the ECM of the host cells or tissue in their native microenvironment (Figure 1.3). The ECM can modulate and regulate the functions of cells by releasing and producing biologically active molecules. This allows the facile modulation of cells and their behavior, as biological, mechanical, developmental and pathological responses can be altered greatly through external cues that occur in the cellular milieu [102].

Another critical characteristic of nanomaterials used for ECM mimicry is porosity. Cells in their native microenvironment are found in a highly ordered and ultracomplex structure at the nanoscale, including different sizes of pores and fibers. Consequently, to guide regeneration and provide proper cell distribution in 3D-scaffold, materials should be engineered in terms of these design criteria.

ECM hydrogels have porous and hydrated structures, making them promising alternatives for mimicking the native microenvironment of cells. Self-assembled peptide nanofiber gels are one example of hydrogels and can be used for nerve regeneration due to their ease of modification and capacity to maintain cells or any soluble factors in a liquid environment. Biologically active molecules can be used for the surface modifications of hydrogels to enhance their biocompatibility and establish a variety of interactions between the material-cell/tissue interface, creating a matrix similar to the ECM of nervous tissue. Long nerve gaps have been treated by using hydrogels containing collagen I and laminin to promote axonal regeneration in peripheral nerve injuries [103].

Studies about tissue engineering are mainly focused on the synthesis of polymers and proteins as scaffolds [104]. Furthermore, these biological scaffolds can be designed innovatively to promote and regulate cell differentiation, proliferation and adhesion without adding any animal-derived factors to the material. This new approach is also used for nerve tissue engineering. This design technique depends on the optimization of the topographical, mechanical, biological and chemical properties of the scaffold to enhance the proliferation and elongation of axons.

Mimicking the ECM by using biomaterials is an effective means to control and direct neural growth and adhesion. This modified microenvironment can be promoted by co-culture technique with cells such as endothelial cells, Schwann cells or oligodendrocytes, and studies have demonstrated major enhancements in neural adhesion, axonal outgrowth and myelination of axons under such conditions [105, 106].

Complex tissues include different types of cells that require a precise set of cell-cell and cell-matrix interactions to continue their function, which can be provided by nanotechnology in a 3D scaffold. The use of nanotechnology allows the implantation of nanoscale cues in scaffolds, which can greatly alter the behavior of cells and enhance a given tissue's capacity for regeneration. However, nanofiber scaffolds are largely under-researched materials for tissue engineering applications, and further research is required to realize their full potential. For ECM applications, the most effective nanofiber scaffolds are typically fabricated using three methods: self-assembly, electrospinning and phase separation.

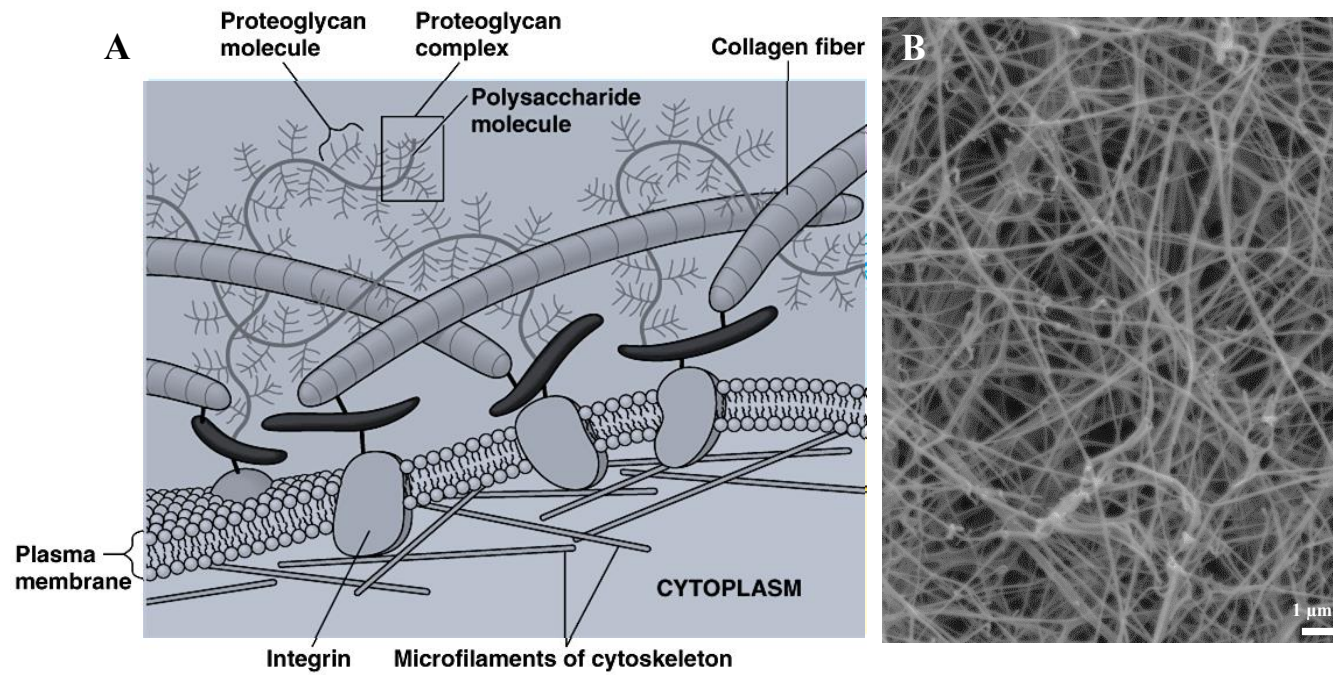


**Figure 1.3.** An illustration of the extracellular matrix, consisting of collagen fiber bridges that extend over cells through integrins located on the plasma membrane (A). Scanning electron micrograph of self-assembled nanofiber scaffold (B) mimicking the native ECM. Reproduced with permission from Pearson Education, Inc., publishing as Benjamin Cummings.

## **1.4. SELF-ASSEMBLED PEPTIDE NANOFIBERS AS SCAFFOLDS FOR PERIPHERAL NERVE REGENERATION**

Self-assembly is an inspirational characteristic of nature and allows the design of new materials as bioactive scaffolds through a bottom-up approach. Many complex tissues and scaffolds can be produced by mimicking self-assembled peptide nanofibers and their hierarchical order, which allow these materials to form highly complex scaffold systems. In addition, peptide amphiphile building blocks can be synthesized chemically using commonly available chemical methods. A broad variety of PA types can self-assemble into micelles, high-aspect ratio nanofibers and various other morphologies under specific conditions. The final structure of the PA assembly can be controlled by modulating the kinetics of the assembly mechanism through changes in pH, temperature and solvent exposure. Peptides are short sequences and functional building blocks that can be used to design biodegradable and biocompatible nanostructures for regenerative medicine applications. The sequence of peptide amphiphile molecules can be determined according to the requirements of the cell type and tissue of interest. Mimicking the biological, chemical and mechanical properties of the natural ECM is the best route for developing novel materials for various applications.

Peptide amphiphiles generally have 4 different regions: a hydrophobic region that contains specific alkyl chains attached to the peptide sequence, a  $\beta$ -sheet forming region that contains 4-8 hydrophobic amino acids (such as valine and alanine) directly

adjacent to the alkyl chain and is important for determining the mechanical properties of the nanofiber gel [107], a charged amino acid region for good solubility and ease of purification, and lastly a bioactive epitope region that contains a peptide sequence intended to emulate some function of the natural ECM of the tissue of interest [108] (Figure 1.4).

The assembly of peptide amphiphiles depends on three important driving forces: the electrostatic interactions between oppositely charged groups, hydrogen bonding among  $\beta$ -sheet forming peptide sequences and the hydrophobic interactions of the alkyl chains. In an aqueous environment, individual PA molecules form PA nanofibers where the hydrophobic core contains alkyl chains trapped in nanofibers and the hydrophilic periphery presents the bioactive epitopes to the external environment without altering the cylindrical geometry of PA nanofibers.

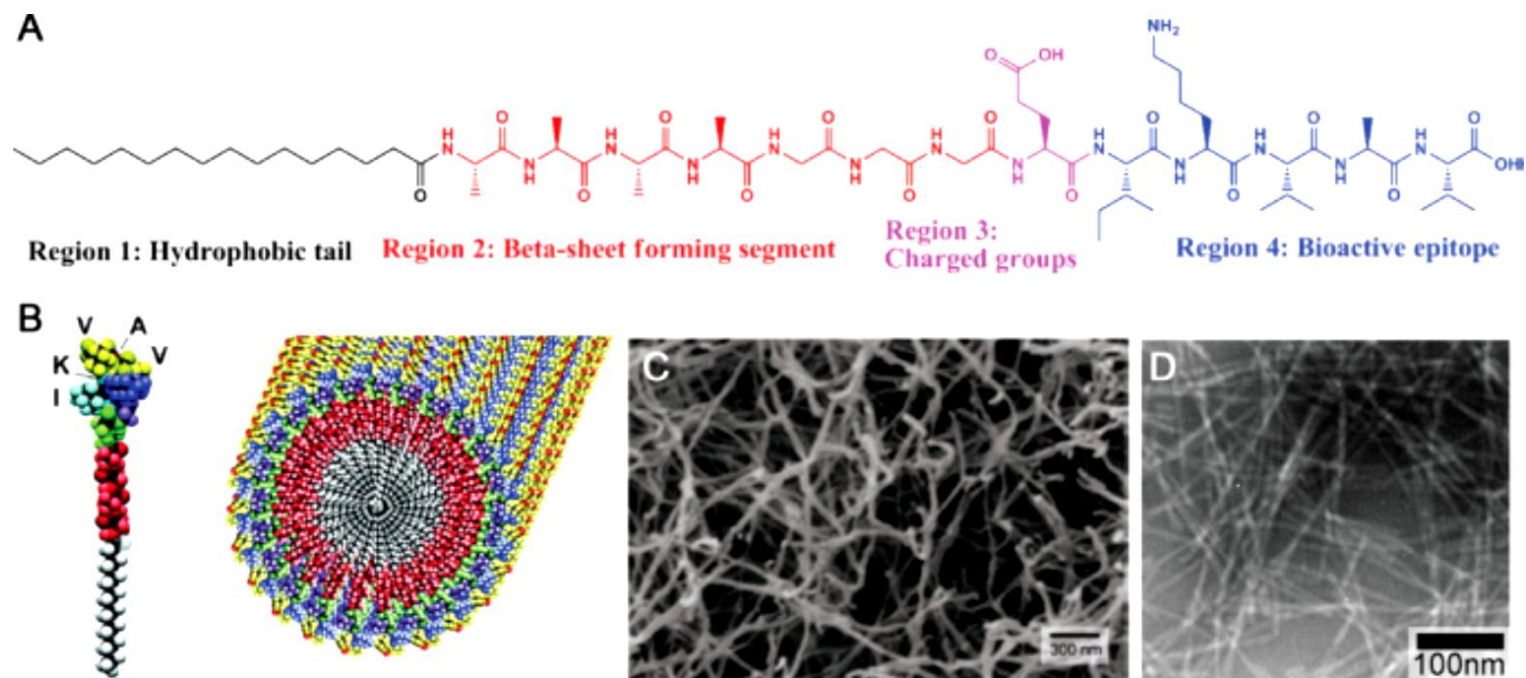


**Figure 1.4.** Chemical structure of an IKVAV-PA molecule, showing four different regions (A). Graphical illustration of peptide amphiphile molecule and its self-assembly into a complex nanostructure (B). SEM image of a peptide nanofiber scaffold demonstrates the similarity of the network structure to the natural ECM (C). TEM image of IKVAV nanofibers (D). Copyright © 2001 American Association for the Advancement of Science. Reproduced with permission from Ref. [109].

The structure of peptide amphiphile nanofibers is similar to the fibrous organization of the natural ECM, allowing the former to serve as a suitable replacement for the latter. In addition, PA networks are able to stimulate cell signaling pathways while physically supporting the cells they contain, effectively performing the roles of the ECM. As such, self-assembled PA nanofibers provide both functional and morphological mimicry of the fibrous extracellular matrix. These nanofiber scaffolds can also promote neuronal migration, proliferation and adhesion. There is a number of peptide sequences in the literature for the treatment of peripheral nerve injuries, including RGD (Arg-Gly-Asp), IKVAV (Ile-Lys-Val-Ala-Val), YIGSR (Tyr-Ile-Gly-Ser-Arg, derived from the laminin  $\beta$  chain) and RNIAEIIKD (Arg-Asn-Ile-Ala-Glu-Ile-Ile-Lys-Asp-Ile, derived from the laminin  $\gamma$  chain and primary cell binding domains) [110, 111]. In addition to these peptide sequences, the N-cadherin mimetic sequence HAV (His-Ala-Val) is an important signaling motif in both neurons and glia [110]. Integrins are major components of the cell membrane and play vital roles in the attachment of cells to the ECM, and PA scaffolds are able to emulate these interactions. RGD is one of the most common sequences for biological adhesion, and has been derived from fibronectin [112]. The laminin-derived IKVAV sequence is also important for cell attachment, migration and growth of neural cells [113, 114]. A gradient of IKVAV-containing peptides was also shown to modulate the development of growth cones in DRG neurons [115]. The direction of axonal elongation was slow when faced with the gradient, and the growth cone reversed directions below a certain concentration threshold.

Self-assembled PA nanofiber gels also function as platforms for the encapsulation, controlled release and delivery of small hydrophobic molecules. A number of

therapeutic drugs and molecules can be incorporated into PA gels to provide biofunctionality, enhance bioactivity and reduce the immune response. Dexamethasone, an anti-inflammatory drug, was loaded into PA gels for controlled release and shown to reduce the immune reaction [116]. Furthermore, PA gels can be used as a gene delivery platform, *e.g.* for antisense oligonucleotides as a novel approach for gene therapy [117]. Hedgehog signaling pathway is also important in nerve regeneration following injury, and sonic hedgehog homolog (SHH) protein plays a critical role in this pathway. SHH-incorporated PA gels were shown to decrease apoptosis and promote nerve regeneration after cavernous nerve injury [118].

## CHAPTER 2

### SCIATIC NERVE REGENERATION INDUCED BY GLYCOSAMINOGLYCAN AND LAMININ MIMETIC PEPTIDE NANOFIBER GELS

This chapter of thesis is partially submitted in the following article; “Mammadov, B., Sever, M., **Gecer, M.**, Zor, F., Ozturk, S., Akgun, H., Ulas, U.H., Guler, M.O., and Tekinay, A.B., *Sciatic Nerve Regeneration Induced by Glycosaminoglycan and Laminin Mimetic Nanofiber Gels*. Acta Biomaterialia, 2016.”

## **2.1. INTRODUCTION**

Peripheral nerve lesions often lead to loss of motor and sensory function of affected area in patient' body need to be reconstructed by surgery. In Europe, over 300,000 people have accidents resulting in PNI and the number of these cases increase every year [119]. These injuries effect the patients' lives negatively socio-economically. Many patients require medical operations for treatment and usually a second operation is inevitable. More than 100,000 patients have an operation because of PNI in US and Europe according to the survey in 2006 [5]. Defects occurred in motor and sensory functions result in the disability of affected limb and neuropathies causing long-term disability. In contrast to long nerve gap, nerve injury with a short nerve gap can be treated by end to end coaptation, but numerous obstacles hamper functional recovery and axonal regeneration. Target organ atrophy and errors in regeneration cause the denervation of the targets and devastating alteration in proliferation, regeneration and production of myelin sheaths of Schwann cells.

Different types of microsurgery techniques are used for the treatment of PNI. These are direct repair (end to end suturing), grafting techniques, (autograft/allograft transplantation) and hollow nerve guidance conduits (NGCs) [27-30]. Deformed nerve gaps can be regenerated by themselves or by using end to end coaptation technique when nerve gap length is less than 1 cm, but long nerve gaps which are 1-5 cm in length can be treated by autograft or allograft (implantation of cadaveric nerve) transplantation methods. Autograft technique is accepted as 'the gold standard'; however, donor site morbidity, neuroma formation, target organ atrophy and

neuropathic pain can occur after applying this technique [120]. Although every other person can recuperate by autograft transplantation operation [106], this nerve grafting technique has been the most preferable for PNI treatment. This successful outcome is owing to the presence of Schwann cells and basal lamina of endoneurial layers. These two factors play an important role for supplying neurotrophic factors and adhesion moieties located on endoneurial layer to promote axonal regeneration. The use of allograft transplantation technique has an advantage to provide an internal scaffold in a 3D manner for Schwann cells and axons; however, the cadaveric transplant can cause immunological response by transferring pathogens to host. As an alternative to these techniques, hollow nerve guidance conduits are more recently researched and used as a template for cell culture and the three dimensional microenvironment for cell adhesion, growth and orientation. NGCs are used for promoting successful regeneration in both the CNS and PNS. These conduits can function as a guidance channel for axon sprouting from the regenerating nerve site, proximal nerve stump, a barrier for infiltration of fibrous tissue, and a permissive environment for neurotrophic factors secreted by Schwann cells at injury site [45]. In spite of functional recovery in PNI, hollow NGCs cannot reach to regeneration level of autologous nerve grafting method [121]. This poor functional outcome resulting from the use of hollow tubes can be overcome by designing biomaterials to modify and functionalize hollow NGCs. Functionalization of hollow NGCs has emerged as an alternative to the autologous nerve grafting technique. This strategy should have properties that allow regeneration of injuries and reconstruction of damaged tissues, and also better mimic of PNS. Especially, internal surface of conduits can be modified by multiple molecules, including neuroinductive moieties, physical guidance cues and neurotrophic factors.

Currently, self-assembled peptide amphiphiles are able to accomplish these design concerns and also perfect candidates for biofunctionalization of nerve conduits. Peptide amphiphiles (PAs) can spontaneously self-assemble into nanofibers due to their molecular multifunctionality including hydrophobic and hydrophilic characteristics with the additional property of presenting biologically active moieties on the external surface of nanofibers [109].

In this thesis, I investigated the use of peptide nanofiber gels filled in polymeric NGCs for peripheral nerve regeneration by using histological analyses and transmission electron microscopy. Peptide amphiphiles were designed to form nanofibers as scaffolds presenting bioactive epitopes associated with nerve regeneration including amino acid sequences derived from laminin and mimicking heparan sulfate. LN-PA molecules, which carry IKVAV sequence, has been shown to promote neurite outgrowth and play an important role in improvement of peripheral nerve regeneration [75]. Laminin is mainly secreted by Schwann cells, required for proper myelination and its disturbance causes inappropriate Schwann cell differentiation and hypomyelination [82]. Highly glycosylated HSPGs are naturally found in basement membrane of neural cells. Both the core protein and glycosaminoglycans (GAG) moieties of HSPGs are known as receptors for growth factors [83, 84]. Especially, bFGF binds to GAG moieties on HS, and bFGF is protected from proteolysis owing to this binding [85]. As well as bFGF, Schwann cells release various types of growth factors that enhance axonal regeneration and control the proteolysis mechanism of neurotrophic factors [45]. Dual effect of LN-PA and GAG-PA nanofiber gels on improvement of neurite outgrowth has been shown *in vitro* [122]. *Neurolac*<sup>®</sup> TW

hollow polymeric nerve conduits were used and functionalized with peptide nanofiber gels and fully transected sciatic nerve model was investigated as *in vivo* model.

## **2.2. MATERIALS AND METHODS**

### **2.2.1. Materials**

9-fluorenylmethoxycarbonyl (Fmoc) and tert-butoxycarbonyl (Boc) protected amino acids [4-[a-(20,40-dimethoxyphenyl)enoxy]acetamidonorleucyl-MBHA resin (Rink amide MBHA resin), Fmoc-Glu(OtBu)-Wang resin and 2-(1H-Benzotriazol-1-yl)-1,1,3,3-tetramethyluronium hexafluorophosphate (HBTU) were purchased from NovaBiochem and ABCR. Dichloromethane (DCM), acetic anhydride, diisopropylethylamine (DIEA), piperidine, dimethylformamide (DMF), trifluoroacetic acid (TFA), triisopropylsilane (TIS) were purchased from Sigma-Aldrich. Toluidine Blue and osmium tetroxide (OsO<sub>4</sub>) were also purchased from Sigma-Aldrich. The other chemicals were purchased from Fischer, Merck, Alfa Aesar or Sigma-Aldrich. Araldite 502 kit was purchased from Electron Microscopy Sciences. All diamond knives were purchased from Diatome. *Neurolac*<sup>®</sup> TW conduits were purchased from Polyganics.  $\beta$ -III-tubulin and S-100 antibodies were purchased from Millipore.

## 2.2.2. Synthesis and Purification of Peptide Amphiphile Molecules

Four different PA molecules were synthesized by solid phase peptide synthesis protocol. LN-PA (Lauryl-VVAGKKIKVAV-Am), GAG-PA (Lauryl-VVAGEGD ( $\rho$ -sulfobenzoate)-Am) and K-PA (Lauryl-VVAGK-Am) were synthesized on Rink amide MBHA resin, only E-PA (Lauryl-VVAGE) was synthesized on Fmoc-Glu(OtBu) Wang resin. During the synthesis; Fmoc protected amino acids, Rink Amide resin for solid support and HBTU for activation of protected groups of amino acids were used. The removal of Fmoc protecting group was performed by 20% piperidine/dimethylformamide (DMF) solution for 20 min. Coupling reaction of 2 mole equivalents of Fmoc protected amino acids was performed by 1.95 mole equivalents of HBTU, and 3 mole equivalents of N, N-diisopropylethylamine (DIEA) for 1 mole equivalent of functional sites on the solid resin, in DMF solution for 4 h. At the end of each coupling reaction, Kaiser test was used for testing coupling reaction. To prevent coupling from remaining free amino groups, 10% acetic anhydride solution in DMF was used for 30 min. After each step, reaction solution was washed with 3 times DMF, 3 times DCM and 3 times DMF again. Except from other three peptide amphiphile molecules, in order to synthesize GAG-PA, sulfobenzoic acid coupling to side chain of lysine residue was performed. To achieve this reaction, Mtt removal was performed by shaking reaction mixture for 5 min with TFA: TIS: H<sub>2</sub>O: DCM in the ratio of 5:2.5:2.5:90. Cleavage of the peptide molecules from the resins was accomplished with a mixture of TFA: TIS: H<sub>2</sub>O in the ratio of 95:2.5:2.5 for 2 h. The removal of excess TFA was completed by rotary evaporation. After TFA removal,

ice-cold diethyl ether was added to precipitate peptide solution and incubated overnight at -20 °C. Centrifugation was done to completely precipitate peptide molecules, then diethyl ether was poured out of falcons and remained ether was evaporated. Peptide molecules was dissolved in the ddH<sub>2</sub>O and frozen -80 °C, lyophilized for 2-3 days and saved at -20 °C.

Synthesized peptide molecules were characterized by liquid chromatography-mass spectrometry (LC-MS) to determine the purity of the molecules. Agilent LC-MS equipped with Agilent 6530 Q-TOF with an ESI source and Zorbax SB-C8 4.6 mm x 100 mm column was used for positively charged peptide amphiphile molecules. On the other hand, an Agilent Zorbax Extend-C18 2.1 mm x 50 mm column was used for negatively charges peptide amphiphile molecules. LC-MS method was optimized as gradient of water (0.1% formic acid or 0.1% NH<sub>4</sub>OH) and acetonitrile (0.1% formic acid or 0.1% NH<sub>4</sub>OH) that was determined as a mobile phase.

A preparative reverse phase HPLC system (Agilent 1200 series) equipped with a Zorbax SB-C8 (21.2 mm x 150 mm) column was used to purify positively charged PA molecules for acidic conditions while Zorbax Extend-C18 21.2 mm x 150 mm column was used for negatively charged PA molecules for basic conditions. The same optimized gradient of water 0.1% TFA or 0.1% NH<sub>4</sub>OH) and acetonitrile (0.1% TFA or 0.1% NH<sub>4</sub>OH) was used as a mobile phase during purification.

## **2.2.3. Physical, Mechanical and Chemical Characterization of Self-assembled Nanofiber Network**

### **2.2.3.1. Scanning Electron Microscopy (SEM)**

Peptide amphiphile nanofiber networks were visualized by using a scanning electron microscope. Gel solutions were prepared as a 1 wt % concentration and they were oppositely mixed in a 120  $\mu$ L final volume. Gels were incubated at 37 °C for 30 min to enhance gelation process. After obtaining PA gels on the silicon wafers, serial dehydration steps were performed. Samples were incubated by increasing ethyl alcohol concentration as 20%, 40%, 60%, 80%, 90%, 100% for 3 min and lastly, in 100% ethyl alcohol were used for overnight incubation at 4 °C. Gels were dried by using Tousimis *Autosamdri®-815* critical point dryer for 2 h to conserve the network structure. After drying process, samples were coated 6 nm Au/Pd and images were taken using a FEI Quanta 200 FEG scanning electron microscope equipped with ETD (Everhart Thornley Detector) detector under high vacuum.

### **2.2.3.2. Oscillatory Rheology**

Investigation of viscoelastic properties of peptide amphiphile gels was performed by using oscillatory rheology measurements with Anton Paar Physica RM301 Rheometer with a 25 mm parallel plate configuration. PA gels were prepared as 125  $\mu$ L/PA molecules at concentration of 4 mM LN-PA, 4 mM GAG-PA, 4 mM K- PA and 2 mM E-PA dissolved in 0.25 M isotonic sucrose solution. Two oppositely charged PA molecules were mixed and carefully transfer to the center of the plate and incubated

for 15 min. After the system reached a plateau, measurement position was set to 0.5 mm.

#### **2.2.4. Surgical Procedure**

Twenty eight ten weeks old male Sprague-Dawley rats were used for this study. Animals were divided into four experimental groups with seven rats. Full transaction injury was performed and 10 mm nerve tissue was excised. 2.5 mm nerve parts from both proximal and distal parts were inserted into 15 mm nerve conduit, and thus, 10 mm gap was left after suturing. In order to obtain biofunctional LN-PA+GAG-PA gels, 100  $\mu$ L from 4 mM LN-PA and 4 mM GAG-PA were injecting into inert conduits while 100  $\mu$ L from 4 mM K-PA and 2 mM E-PA were injected into inert conduit and used as an epitope-free control. All PA molecules dissolved into 0.25 M isotonic sucrose solution. For non-treated controls, nerve conduits were filled with sucrose and for autograft controls, sciatic nerves were excised then reversed and sutured back to nerve stumps. All surgical operations were performed on the right hind limbs and left hind limbs were used as healthy control. All procedures were approved by Animal Ethics Committee of Gülhane Military School.

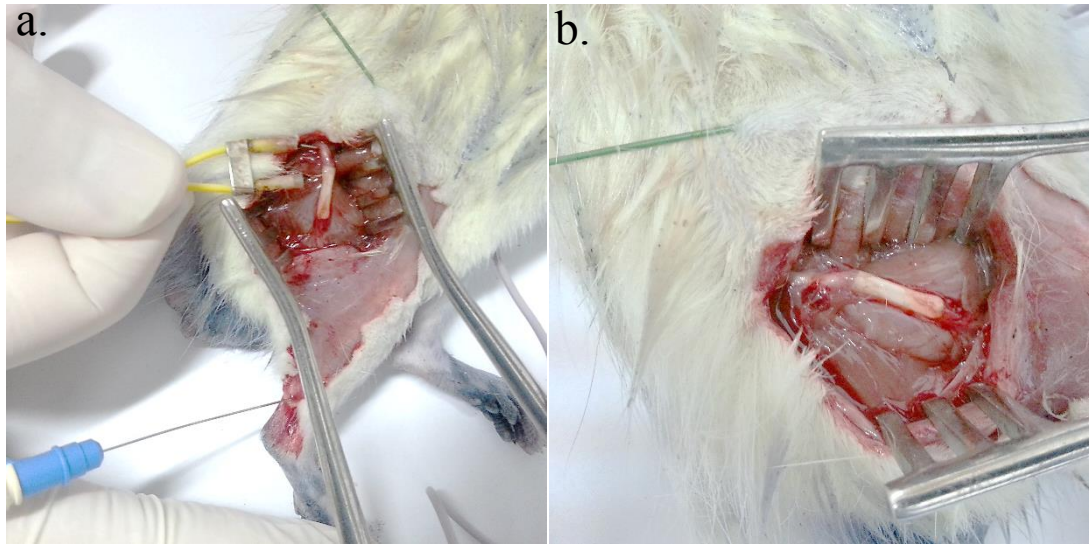


**Figure 2.1.** Images of electrophysiological assessment shows supramaximal stimulus (a) and the location of needle electrodes on soleus muscles (a-b).

### **2.2.5. Electrophysiological Investigation**

The assessment of electrophysiological recovery was investigated by using electromyography (EMG) device. 12 weeks after the surgery, rats were anesthetized by a subcutaneous injection of xylazine (20 mg/kg) and ketamycin (80 mg/kg) then both sciatic nerves were explored. Needle electrodes were placed to soleus muscles (Figure 2.1., b.) and supramaximal stimulus (Figure 2.1., a.) was applied to proximal of the injury sites in rat' s right and left hind limbs to the same place. Data was recorded as latency and amplitude of the sciatic nerve. The recovery of amplitude percentage was calculated by dividing the amplitude of the healthy sciatic nerve to operated amplitudes. Differences of latency was calculated by subtracting healthy sciatic nerve latency from operated.

## 2.2.6. Histological Analysis

12 weeks after the surgery, sciatic nerve tissues were harvested from each animal and tissues were cut into three parts named proximal, mid-tissue and distal. Mid-tissue was a 2 mm fragment dissected from the middle part of the nerve graft and it was fixed in 2.5% glutaraldehyde. Before 2% OsO<sub>4</sub> fixation for 4 h, tissues were rinsed with PBS (1X) for 15 min 2 times. After post-fixation step, serial ethanol exchanges were performed for dehydration. Proximal and distal fragments of the nerve grafts were used for hematoxylin eosin staining (H&E) and immunohistochemistry (IHC) analysis. These fragments were fixed with 10% formalin. After performing dehydration steps with ethanol and xylene exchange, tissues were embedded into paraffin. Sectioning was performed by Leica microtome to obtain 4 µm thick longitudinal sections on the positively charged slides for H&E and IHC experiments. Sections were deparaffinized at 58 °C incubated overnight in oven and rehydrated in serial exchange with decreasing ethanol concentration. For getting nuclei staining, slides were incubated with Mayer's hematoxylin for 45 sec and for counterstaining eosin Y solution incubation used for 50 sec. After staining with H&E, dehydration continued with serial ethanol exchange with increasing concentration and lastly xylene exchanges were performed, slides were mounted with xylene based mounting medium with coverslips.

The slides that were determined according to the results of H&E staining, were deparaffinized for immunocytochemistry by using the same protocol mentioned above. After rehydration step, antigen retrieval was performed with 200 µL pepsin per tissue at 37 °C for 10 min. To remove excess of enzyme, slides were rinsed with running tap

water for 3 min. Before blocking step, slides were washed with TTBS (0.025% Triton-X-100 in Tris- buffered saline) for 5 min, 2 times. In humidified chamber, slides were incubated 200 µl blocking solution (10% normal goat serum (NGS) and 1% bovine serum albumin (BSA) in TBS) per tissue at room temperature for 2 h. Slides were drained and primary antibodies were diluted in TBS with 1% BSA. Sections were stained with anti-β-III-tubulin (1:100, Millipore, 04-1049) and anti-S-100 (1:250, Millipore, 04-1054) overnight at 4 °C. The day after slides were incubated at room temperature for 30 min and rinsed into TTBS for 5 min, 2 times. After primary antibody staining, horseradish peroxidase (HRP)-conjugated goat anti-rabbit secondary antibody (1:500, Millipore, 12-349) incubation was performed for 1 h at room temperature. Slides were washed with TBS for 10 min, 2 times and for 5 min. 3, 3'- diaminobenzidine (DAB) enhanced liquid substrate system was performed to get coloration. After hematoxylin staining, tissues were mounted with xylene based mounting medium and covered with glass coverslips.

### **2.2.7. Ultrastructural Investigation**

Resin embedded tissues were sectioned as 1 µm thick by using Leica EM UC6 ultramicrotome. By using glass strips, sections were collected on water boat and sections were transferred on to glass slide. After the sections completely dried, glass slides were stained for 2 min with the heater. These sections were stained with 1% toluidine blue and 2% sodium borate in distilled water. After dissolving the sodium borate and the toluidine blue powder in the water, the staining solution was filtered using syringe filter. Excess stain was rinsed off gently with distilled water and then

sections let air drying. As a last step, sections were covered with regular clear mounting medium and put the slides to oven 60 °C for 30 min. Images were taken with Zeiss Axio Scope A1 microscope. The numbers of myelinated axons were quantified by using Image J software and the axon numbers from operated tissues were normalized to healthy tissues. For the number of myelinated axons/area quantitation, 3 images were taken with 1000X magnification.

By using ultramicrotome device, ultrathin (80-100 nm) transverse sections were taken with diamond knives and after that uranyl acetate and lead citrate staining were applied. Firstly, sections were stained with 4% uranyl acetate in ddH<sub>2</sub>O for 20 min. After staining, samples were washed with ddH<sub>2</sub>O for 15 sec at 3 times. Before starting lead citrate staining, samples were located in petri dish with couple of NaOH pellets to reduce humidity. Sections were stained with lead citrate (Reynold's lead citrate solution) for 10 min and washed with ddH<sub>2</sub>O for 15 sec at 3 times. All stained sections were left to dry at least 30 min. TEM and STEM images were carried out for a quantification of axon and fiber diameter, thickness of myelin sheath and g-ratio (axon /fiber diameter). The thickness of axons and the diameter of axons and fibers were quantified by using Image J software. Diameters were quantified from images under the assumption that the fibers and axons were perfect circles.

### **2.2.8. Statistical Analysis**

One-way ANOVA analysis with Bonferroni's Multiple comparison test was used for statistical analysis to compare experimental groups.  $p < 0.05$  was considered statistically significant.

## **2.3. RESULTS AND DISCUSSION**

### **2.3.1. Synthesis and Purification of Peptide Amphiphile Molecules**

Tissue-engineered biodegradable artificial nerve guides are chosen to avoid the risks related with non-degradable conduits and severe foreign body reactions [119]. These biodegradable materials provide many advantages, such as Schwann cell migration, secreting or attracting biochemical cues to injury sites by biochemical modifications of conduits. From this point of view, *Neurolac*<sup>®</sup> *TW* nerve conduits were filled with peptide amphiphile nanofiber gels to obtain biologically functional nerve guidance conduits. A pentapeptide, laminin-derived bioactive epitope “IKVAV” incorporated into LN-PA molecules and glycosaminoglycan mimetic GAG-PA molecules that give ability to capture growth factors, such as FGF-2, VEGF and BMP-2 proteins, were used to induce axonal recovery [123].

Four different PA molecules were synthesized by using solid phase peptide synthesis protocol. LN-PA and GAG-PA were designed (Figure 2.2. and Table 1.1.) and synthesized for biofunctionalization of hollow nerve conduits, non-bioactive PA molecules, named K-PA and E-PA, were also used as a control nanofiber gel. All peptide amphiphile molecules have ability to form peptide nanofibers and these four PA molecules consist of 4 different building blocks; a hydrophobic alkyl tail (for this study lauric acid was used), beta sheet forming part (VVAG), peptide charged segment (positively or negatively charged amino acids like lysine in K-PA and glutamic acid in E-PA) and a bioactive epitope part [108]. These building blocks have the capacity

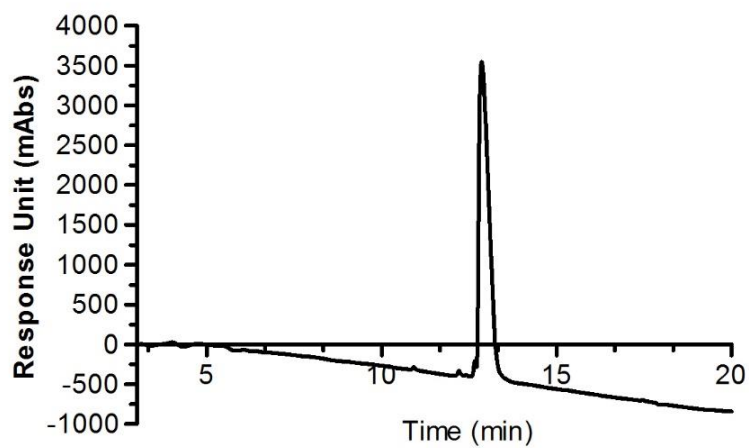
for self-assembly which is triggered by non-covalent interactions such as hydrogen bonding, electrostatic interactions, Van der Waals interactions at the hydrophobic segment and  $\pi$ - $\pi$  stacking [124]. All PA molecules were purified by reverse HPLC or dialysis method and the purity level of synthesized PA molecules was characterized by performing LC-MS (Figure 2.3.-2.6.). According to the mass spectra, the obtained molecular weight of PA molecules are; 1293.035  $[M+H]^+$  for LN-PA, 1224.400  $[M-2H]^-$  for GAG-PA, 654.416  $[M-H]^-$  for E-PA and 654.494  $[M+H]^+$  for K-PA.

<b>Peptide Amphiphile</b>	<b>Sequence</b>	<b>Molecular Weight (g/mol)</b>	<b>Net Charge</b>
LN-PA	Lauryl-VVAGKKIKVAV-Am	1292.74	+3
GAG-PA	Lauryl-VVAGEGD( $\rho$ -sulfobenzoate)-Am	1226	-3
K-PA	Lauryl-VVAGK-Am	654	+1
E-PA	Lauryl-VVAGE	655.82	-2

**Table 2.1.** Sequences, molecular weights and net charge at pH 7 of peptide amphiphile molecules.



A)



B)

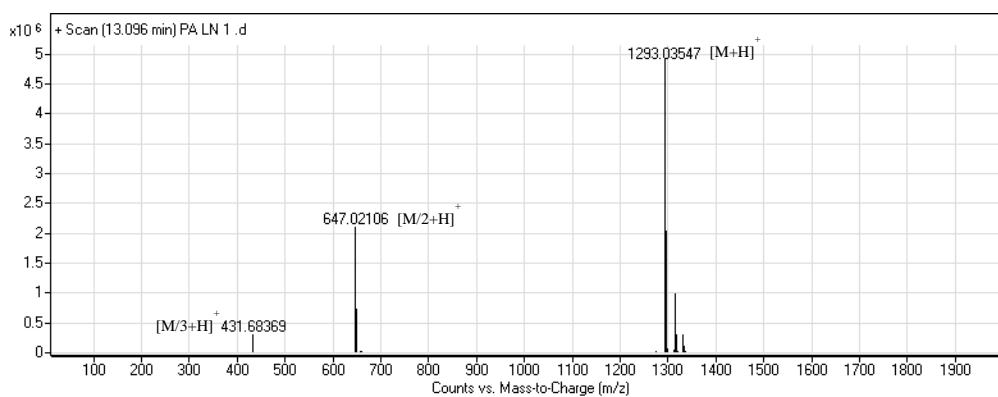


**Figure 2.3.** Liquid chromatography (A) and mass spectrometry (B) analysis of LN-PA.

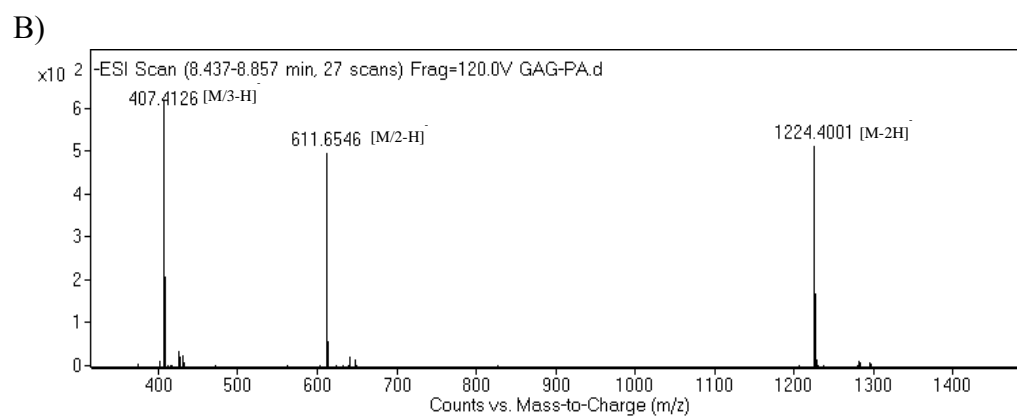
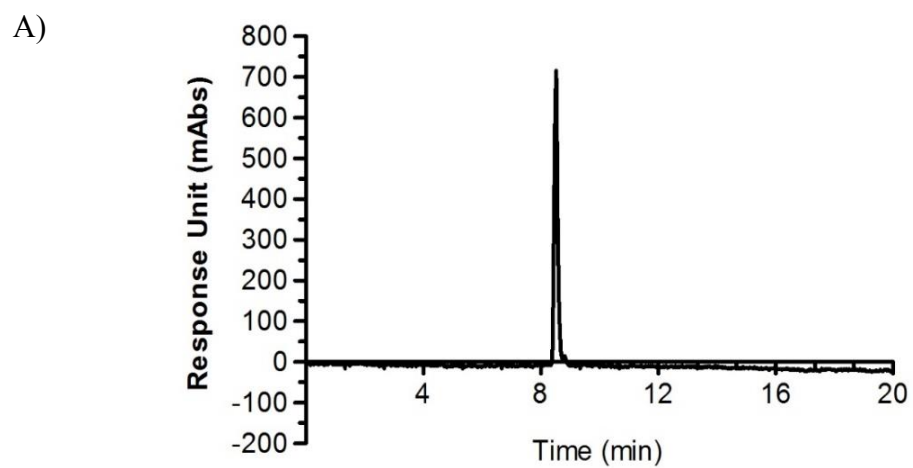


**Figure 2.4.** Liquid chromatography (A) and mass spectrometry (B) analysis of GAG-PA.

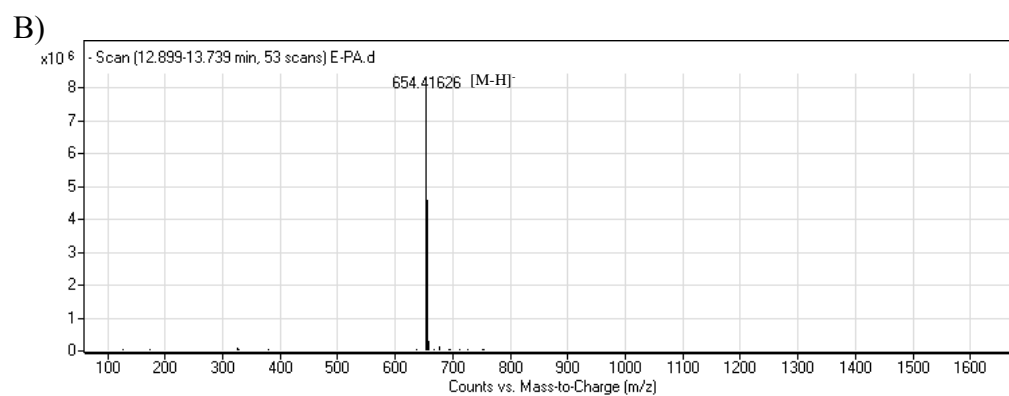
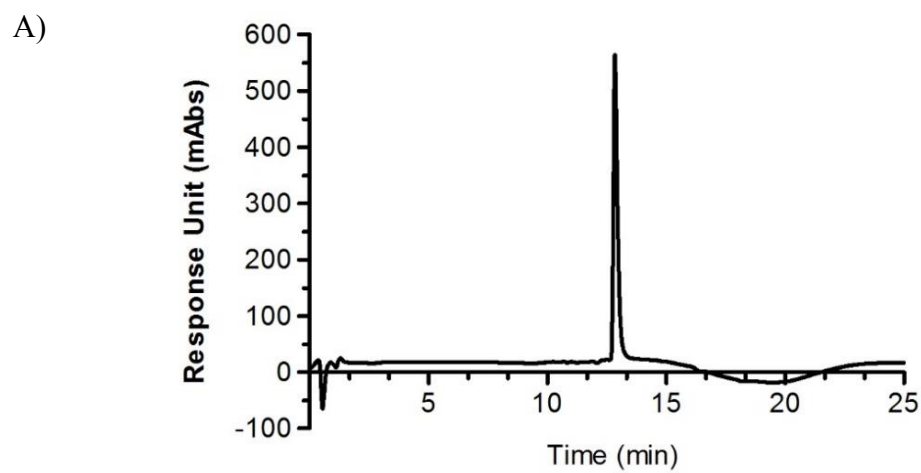


**Figure 2.5.** Liquid chromatography (A) and mass spectrometry (B) analysis of E-PA.

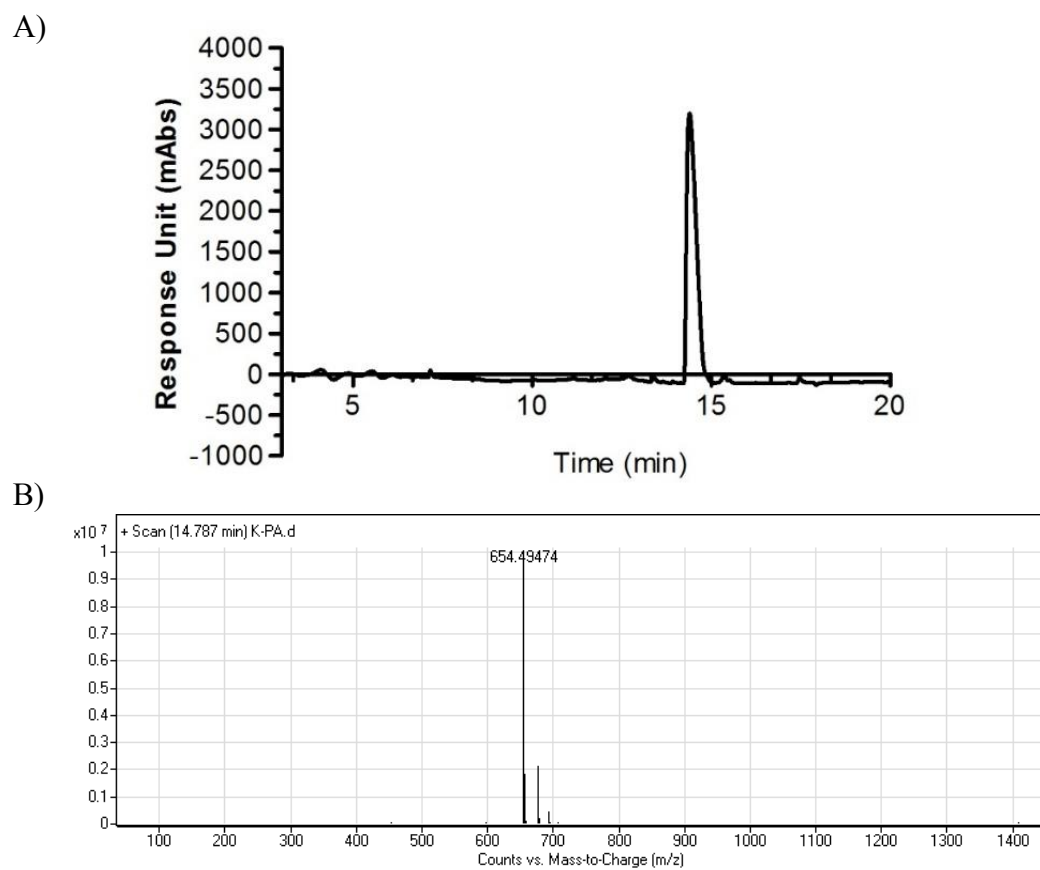


**Figure 2.6.** Liquid chromatography (A) and mass spectrometry (B) analysis of K-PA.

### **2.3.2. Characterization of Peptide Amphiphile Nanofibers**

Self-assembly of peptide nanofiber gels was characterized with using different methods. To reveal the structural characterization of PA nanofibers is essential for understanding cell-material interactions and cell behavior. When two oppositely charged PA molecules were mixed, they self-assemble into nanofibers by charge neutralization, with the help of driving forces coming from the supramolecular properties among the building blocks [125]. There are three major locomotive forces for self-assembly of PAs; hydrophobicity of alkyl tails,  $\beta$ -sheet forming unit of the middle part and electrostatic repulsion and attraction of charged amino acids [108]. Nanofibrous structure of PA gels was characterized by scanning electron microscopy. The SEM images of PA gels (Figure 2.7.) revealed the fibrous formation of PA gels and resemblance to natural ECM nanofibrous structure. The incorporation of native ECM epitopes into the PA networks enables to the structural and functional mimicry of natural ECM. Focal adhesion complexes are one of the examples for this kind of incorporations that are triggered by different peptide epitopes [126, 127].

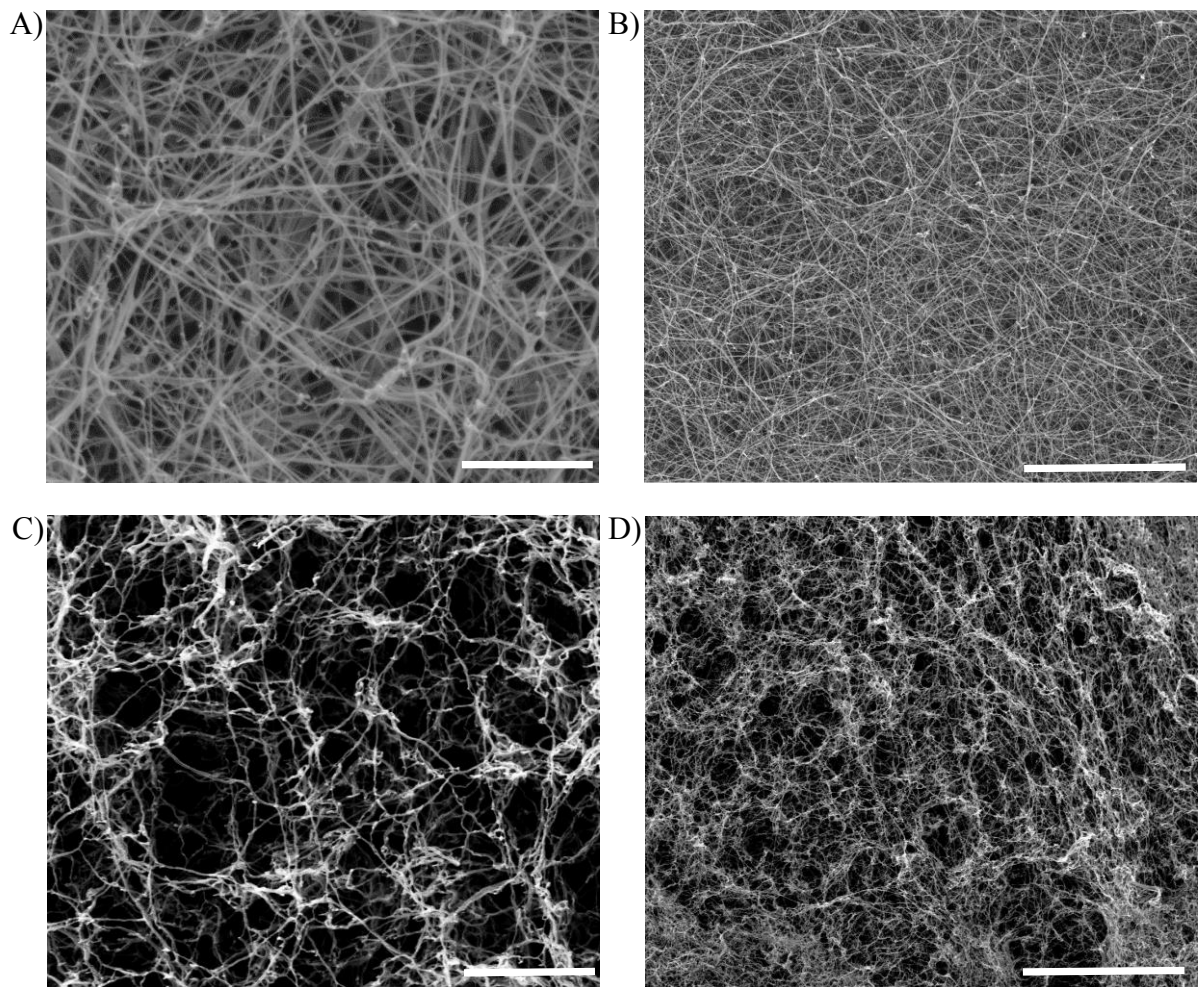


**Figure 2.7.** Scanning electron microscopy images of nanofibrous scaffold PA gels. LN-PA/GAG-PA (**A, B**), and K-PA/E-PA (**C, D**). Scale bars are 1  $\mu\text{m}$  (**A, C**) and 5  $\mu\text{m}$  (**B, D**).

The mechanical properties of synthetic scaffold have major influence on cell fate like migration [128, 129], apoptosis [130] and proliferation [131]. The mechanical stiffness of an artificial ECM is a one of the key physical factors affecting cell responses to scaffold [132]. The elasticity of soft materials was found to be neurogenic when it less than 1 kPa [133]. One of the study in the literature showed that adult neural stem cells were cultured on a hydrogel scaffold varying in elastic moduli between 10 and 10,000 Pa. On soft gels (10 Pa) neural spreading and differentiation were suppressed, but on the scaffolds with elastic moduli of 100 Pa or greater, they reached the peak level of neural differentiation [134]. The oscillatory rheology results show that the value of storage modulus of LN-PA/GAG-PA gel is between 0.1- 1 kPa and K-PA/E-PA gel is close to 0.1 kPa. These PA gel systems are soft enough to enhance to neural attachment and extension.

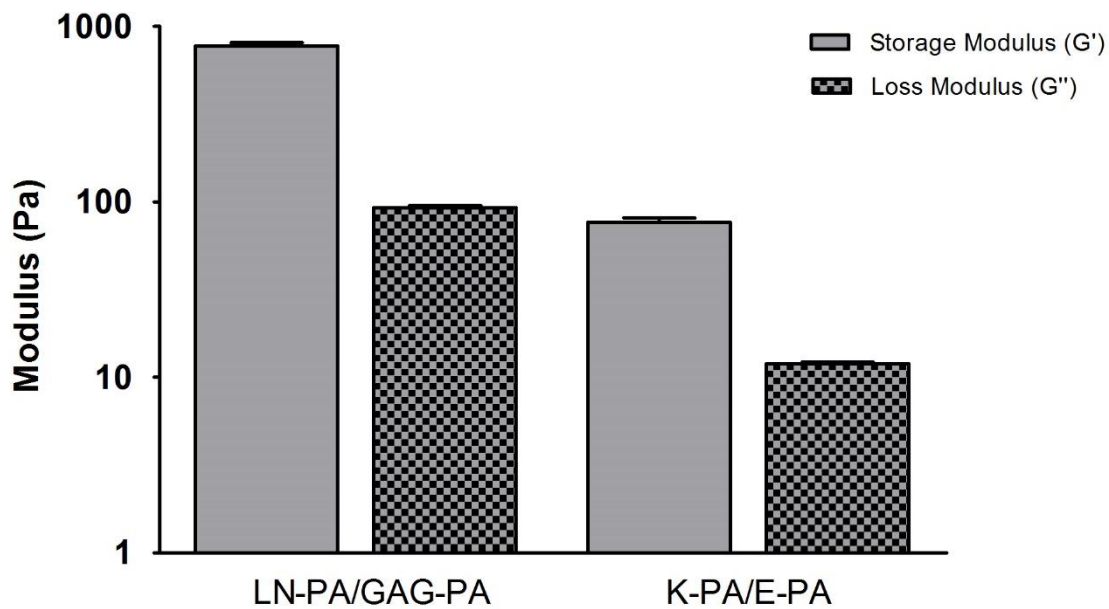


**Figure 2.8.** Storage and loss modulus measurements of peptide amphiphile gels by oscillatory rheology. Rheology results showed that the mixtures of peptide amphiphiles are soft materials suitable for neural tissue applications.

### 2.2.3. Electrophysiological Assessment

12 weeks after the surgery, electrophysiological assessment of the operated sciatic nerve can provide some information about the functional state of the regenerated nerve. Electrical stimuli were applied to the soleus muscles at the proximal site and the distal end of graft sequentially by electromyogram. Post-operatively, amplitudes and latencies of both operated and healthy limbs were detected to evaluate the recovery of nerve segment. Amplitude results show the size of the action potential and latency measurements show the time needed for electrical signals to reach the target organ.

In our study, we demonstrated that LN-PA/GAG-PA bioactive gel system induced the axonal regeneration, the proliferation of newborn neurons and Schwann cells. These results showed that this bioactive gel system injected into *Neurolac*<sup>®</sup> TW conduits could be used in clinics without any negative effects on peripheral nerve regeneration. Electromyography results showed that the recovery level of electrophysiological properties in conduits biofunctionalized with LN-PA/GAG-PA gels was significantly better than sucrose treated conduits and autograft treatment group, but the difference was not significant with K-PA/E-PA treated group (Figure 2.9). K-PA/E-PA group also showed better amplitudes than sucrose and autograft groups. However there was no significant difference in the amplitude. In addition to the success of amplitude recovery, latency measurements indicated that the signal transmission is faster in peptide nanofibers treated groups relative to sucrose and autograft treatment groups (Figure 2.10). However, there was no significant difference among the groups in terms of the latency. This result revealed that transmitted signals reached to the target organ faster when the conduits were filled with PA gels.

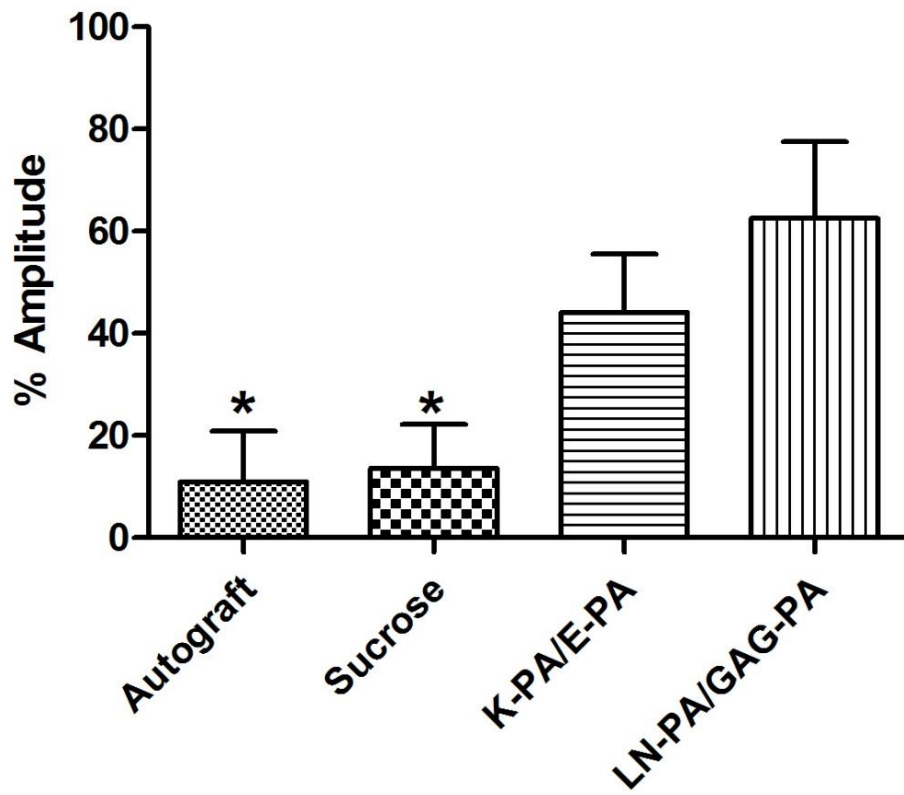


**Figure 2.9.** Functional evaluation of transected nerve via measurement of the amplitude.

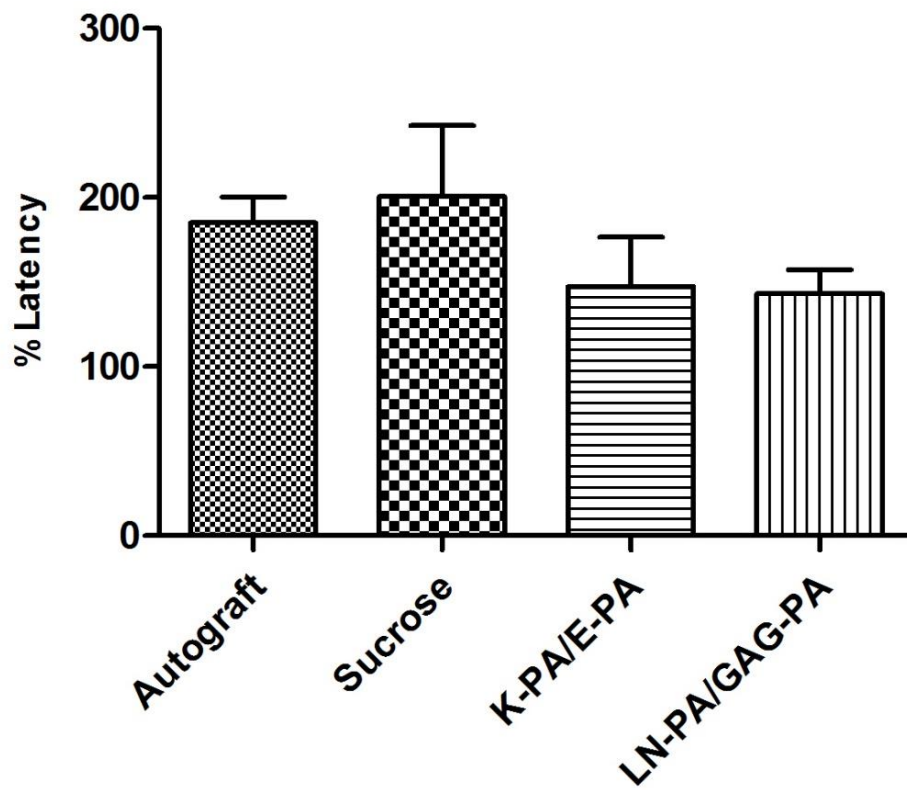


**Figure 2.10.** The results of evoked potential at 12 weeks after surgery.

#### **2.2.4. Histological Assessment of Sciatic Nerve Tissues**

The basic structural characteristic of peripheral nerve fibers represents the infrastructure for its guidance of regeneration in injuries, especially for full transection. The outer layer of a regular nerve fiber, epineurium covering peripheral nerve, sustains the integrity and incorporation with its surrounding tissues, while the inner layer of nerve fiber, nerve fascicles, maintains the guidance of axonal elongation, proliferation and function. The natural extracellular matrix components, especially laminin and heparan sulfate glycosaminoglycans, have an essential role for cellular bioactivity. Particularly, these ECM molecules stimulate cell migration and proliferation of Schwann cells and have an effect on axon growth cones [135].

The newly developed nerve conduits for transected nerve tissues have been widely studied by lots of researchers in order to guide axonal growth from proximal end to distal end. However, the length of gap between proximal stump and distal stump is a challenging factor causing inadequate axonal guidance which results in limited number of axons reaching to the distal part. Empty polymeric nerve conduits are just hollow tubes that only provide an isolation of the injured nerve sites from surrounding tissue and a physical guidance to regenerating axons. Besides, the absence of biochemical modifications of these nerve conduits prevents the Schwann cell and neuron migration, proliferation and attachment.

Currently, commercially available empty polymeric nerve conduits are used for treatment of peripheral nerve injury. For this kind of treatments, transection gap should be between 1 cm to 3 cm [136].

The full transection of rat sciatic nerve model is a widely used and approved peripheral nerve injury model [137]. In this study, 10 mm full transection of sciatic nerve model was performed and 15 mm nerve conduits were sutured to transected nerve ends.

The biofunctional activity of laminin derived IKVAV (Ile-Lys-Val-Ala-Val) bioactive peptide sequences was demonstrated in spinal cord injury studies [138, 139]. This integrin binding sequence interacts with cell membrane through integrin receptors and plasma membrane molecules. Also laminin molecules critically contribute to cell attachment, proliferation and secretion of biochemical cues by Schwann cells. The other important bioactive signal used in this study is heparan sulfate glycosaminoglycan mimetic peptide sequence that binds to growth factors and cell surface receptors. This bioactive signal was used to induce axonal growth and the secretion of growth factor binding molecules from Schwann cells. The effect of LN-PA/GAG-PA on functional recovery of full transection sciatic nerve injury model was evaluated 12 weeks after injury.

At 12 weeks, truncated sciatic nerve specimens were harvested for detailed analysis to evaluate the impact of LN-PA/GAG-PA on regenerating peripheral nerves. For peripheral nerve studies, presenting of the various components of peripheral nerve tissue is really important to understand the effect of the treatment. Generally, selecting specimens is substantial from different part of the characteristic structure of peripheral nervous system, when studying peripheral nerves. It is important to harvest specimens from proximal and distal segment of nerves, since axonopathies and neuropathies frequently impair more distal parts than proximal parts. Longitudinal sections of regenerated sciatic nerves were stained with H&E (Figure 2.11), anti-S100 antibody

for Schwann cells (Figure 2.12) and anti  $\beta$ -III tubulin to evaluate the neural regeneration (Figure 2.13). In our study, we demonstrated that LN-PA/GAG-PA bioactive gel system induced the axonal regeneration and the proliferation of newborn neurons and Schwann cells. The histological assessment revealed that only peptide nanofiber treated groups reached from the proximal to the distal end (Figure 2.11). The axonal arrangement in all groups was similar to the healthy tissue at the proximal site. Under higher magnification, it was clearly seen that the density and the linearity of the regenerated axons were better in LN-PA/GAG-PA treated group than K-PA/E-PA treated group. Only a few axon fibers reached to the distal stump and the linearity of the elongated fibers were rarefied in sucrose filled group.

The linearity of axons was obviously good in all treatment groups in proximal part, but only in peptide nanofiber applied groups showed the better linear structure in distal end. This means that nanofiber network provides axonal guidance to reach the distal end. The hallmarks of Wallerian degeneration can be clearly seen at the distal part of all treatment groups except LN-PA/GAG-PA treated group. The arrangement of the axon fibers was diminished in the distal segment in all treated groups except LN-PA/GAG-PA group, but this linearity was not as good as at the proximal site. It means that LN-PA/GAG-PA bioactive gels promote proliferation of myelinating Schwann cells and secretion of soluble factors for attracting macrophages to the injury site by inducing laminin-integrin signaling. After collagen, laminins are the most common ECM proteins in the peripheral nervous system, that promote axonal elongation. There are 15 laminin trimers found in basal lamina, but only two types of laminins are expressed in PNS (Laminin 2 and Laminin 8) [15], and their expression levels are enhanced after PNI [140]. Laminins have strong influence on Schwann cells and

neurons via binding to integrins that boost the cell adhesion, myelination and axonal outgrowth [141-143]. For example, knockout of the  $\gamma 1$  laminin subunit in Schwann cells exceedingly inhibits axonal growth and changes the Schwann cells' physiology such as delays in proliferation and axon ensheathment [77]. Also macrophages have a primary role in the removal of debris and production of trophic factors in the next stage of Wallerian degeneration. Thus, GAG mimetic bioactive gels aid the macrophages by binding growth factors (e.g. FGF-2) [144].

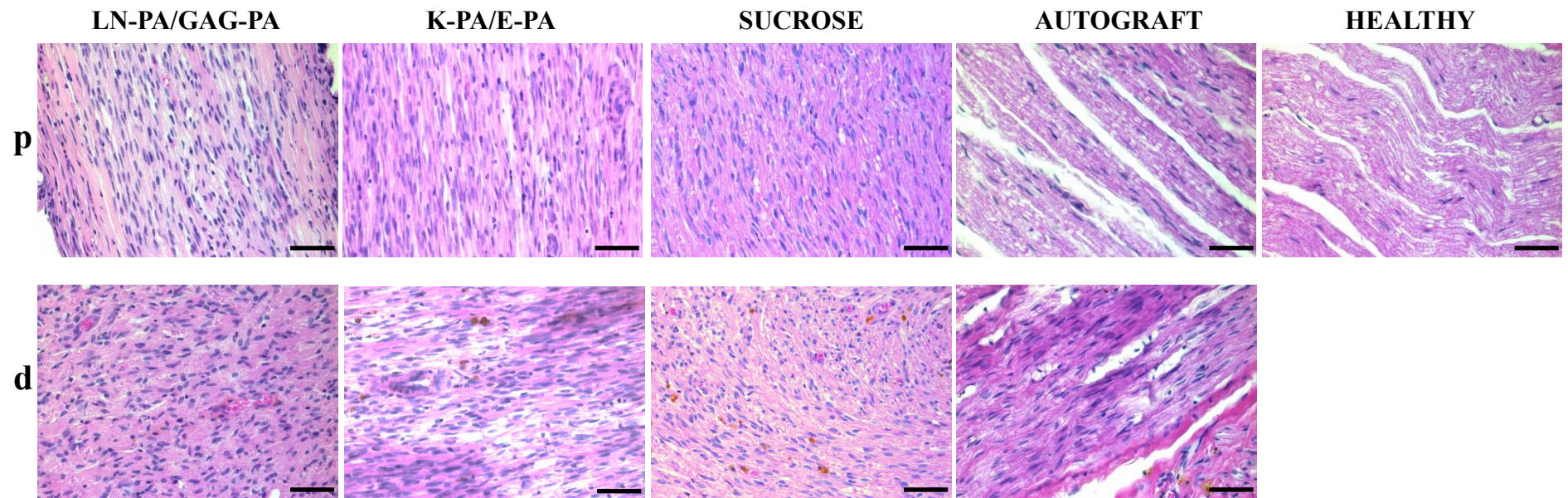


**Figure 2.11.** Hematoxylin & Eosin (H&E) staining of sciatic nerve tissue specimens: (**p**) proximal, (**d**) distal. Scale bars are 50  $\mu$ m.

Schwann cells are one of the major components of the peripheral nervous system, are important for nerve function, and 90 percent of nucleated cells of PNS is comprised of them [145]. Myelinating and ensheathing Schwann cells are found in PNS and myelinating Schwann cells assist transmission of an action potential through axons rapidly by providing insulation. Schwann cells induce axonal regeneration and elongation by providing extracellular matrix molecules, growth factors and tropic factors [14]. In the distal part of the peripheral nerve, Schwann cells secrete trophic factors that attract immune cells into the damaged area [146]. Sciatic nerves were stained with anti  $\beta$ -III tubulin antibody and anti S-100 antibody to obtain deeper information about the state of the regeneration. The staining of S-100 was performed to evaluate the regeneration and the repopulation of Schwann cells in the newborn nerve and at the injury site. This evaluation is a significant cue for regenerated and properly myelinated axons. We have demonstrated that the intensity of S-100 staining increased when conduits were filled with bioactive PAs (Figure 2.12). Schwann cell population in the proximal segment of nerve was similar in H&E and S-100 staining of all treatment groups. In distal segment, the highest population of Schwann cells was observed in LN-PA/GAG-PA treated group. Schwann cells should be placed properly at the distal segment of nerve tissue for sufficient myelination and healthy signal transmission from the proximal to the distal site of the graft. This placement of Schwann cells along the axons is quite different from the healthy tissue in autograft treated group at the distal site.

$\beta$ -III tubulin staining indicated that axonal regeneration is remarkably better in LN-PA/GAG-PA treated group than the other three groups (Figure 2.13). At the proximal site, S-100 and  $\beta$ -III-tubulin staining patterns in autograft treated group were very

similar to healthy tissue, for the distal part these staining patterns were different from the healthy one. A higher number of  $\beta$ -III-tubulin-positive axons can be clearly seen in proximal part of bioactive PA treated group. The intensity of  $\beta$ -III-tubulin staining and the distribution of  $\beta$ -III-tubulin-positive axons were better in the presence of bioactive PAs relative to the other treatment groups in the distal segment. This indicates that more axons elongated and reached to the distal part from the proximal part of truncated sciatic nerve. This staining proved that the axonal regeneration was observed not only at the proximal site but also at the distal site of the injury site. The deficient innervation and insufficient arrangement in the distal stump were observed for K-PA/E-PA, sucrose and autograft treated groups and the results of  $\beta$ -III-tubulin are compatible with the H&E staining.

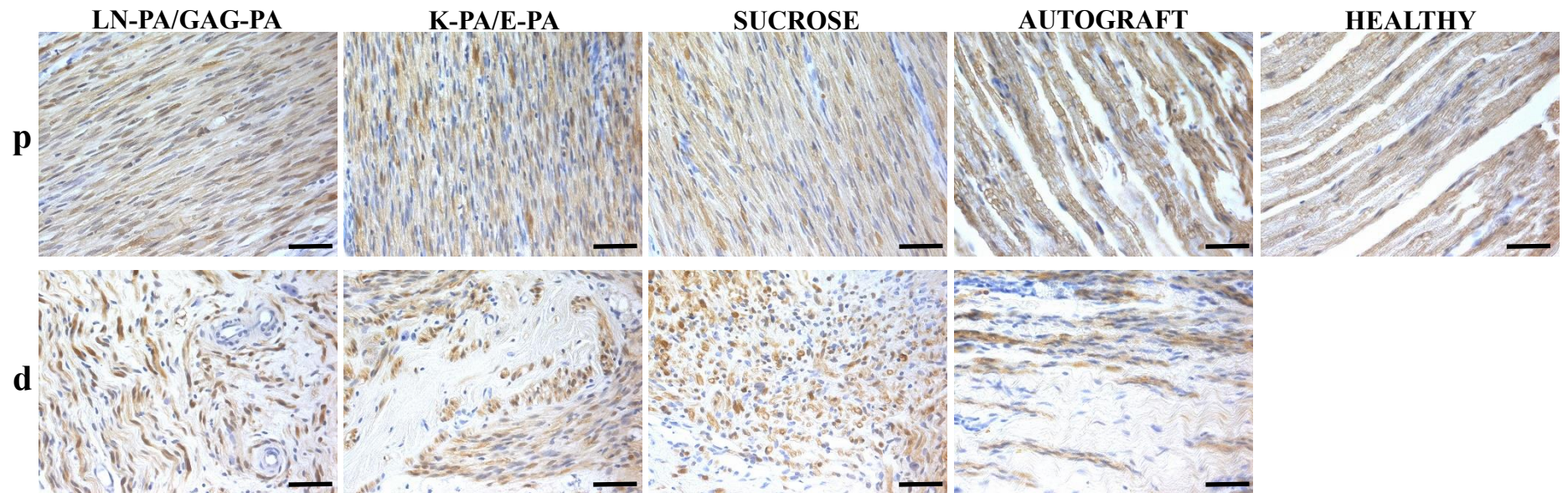


**Figure 2.12.** Immunohistochemical staining of sciatic nerve tissue specimens with anti S-100 antibody: (**p**) proximal, (**d**) distal. Scale bars are 50  $\mu$ m.

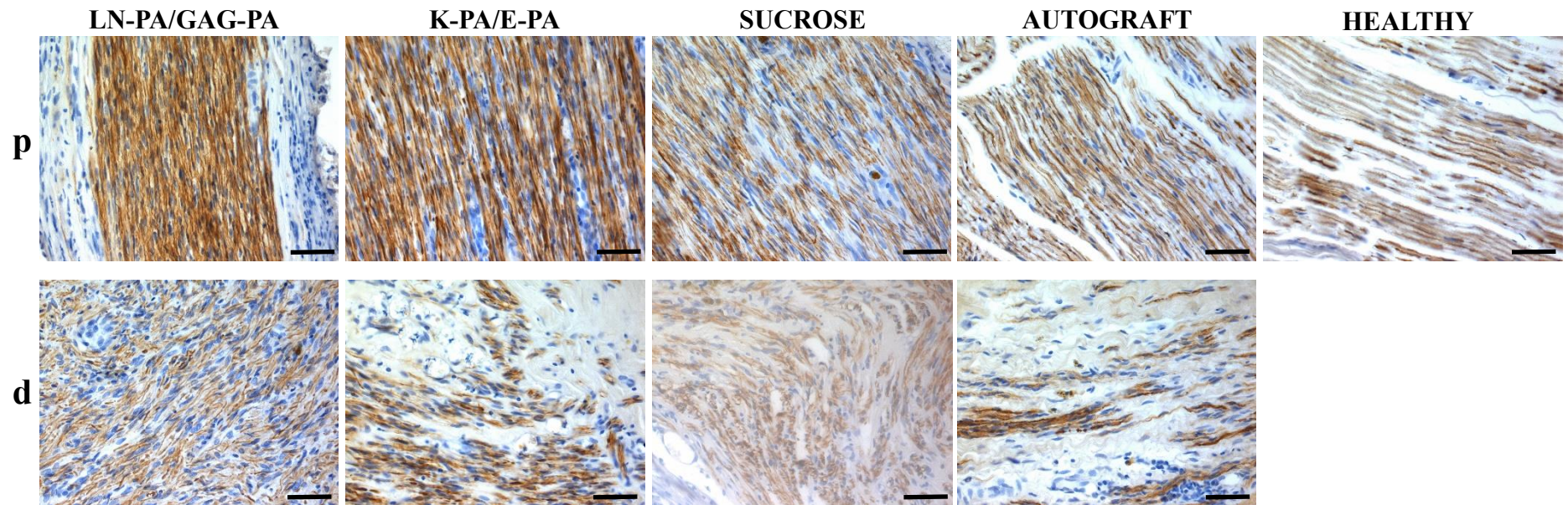


**Figure 2.13.** Immunohistochemical staining of sciatic nerve tissue specimens with anti  $\beta$ -III-Tubulin antibody: (**p**) proximal, (**d**) distal. Scale bars are 50  $\mu$ m.

### **2.2.5. Ultrastructural Assessment of Nerve Regeneration**

Detailed histological assessment of functionalized nerve conduits is beneficial for assessment of ordered structure, axonal elongation, remyelination, axon density and integrity. Paraffin-embedded proximal and distal nerve segments sectioned longitudinally are helpful to see the denervated tissues in such histological analysis method. However, this preparation did not provide the resolution of resin embedded sections. Consequently, to go deeper in analyses of the morphological structure the regenerating nerve tissues, toluidine blue-O stained transverse semi-thin sections were analyzed by light microscopy at high magnification and ultrathin sections were analyzed by transmission and scanning transmission electron microscopy.

The morphology of all treatment groups was shown in toluidine blue-O stained tissues (Figure 2.14-17). LN-PA/GAG-PA treated group showed the most similarity to healthy nerve tissue morphology when compared to K-PA/E-PA treated, sucrose treated or autograft groups (Figure 2.14). The presence of Schwann cells indicates that the proper myelination, regeneration and axonal elongation in damaged nerve tissues could proceed via bioactive hydrogel filled nerve conduits. It is most clear in bioactive PA gel treated group that Schwann cells were highly populated the mid part of the conduits relative to the other treatment groups (white arrows) and this result is in good correlation with S-100 staining. The continuity of Schwann cells on axons is very important for the reconstruction of the nerve signal transmission.

Especially in LN-PA/GAG-PA filled conduits, distribution of nerve fibers was more homogenous than K-PA/E-PA filled conduits. Abnormal morphology of axons can be clearly seen in K-PA/E-PA treated group (Figure 2.15).

In addition, undefined morphological structures were observed in sucrose treated group (black arrows) (Figure 2.16). The morphological examination of autograft treatment group revealed that Schwann cells were surrounded by onion-bulb like structures and several stages of demyelination (white arrows) (Figure 2.17). The morphologically closest group to the healthy nerve tissue structure was LN-PA/GAG-PA, and morphometric analysis revealed that there was no significant difference regarding the density of myelinated axons (Figure 2.18). However, quantitative analysis showed that the number of myelinated axons was higher in both sucrose and LN-PA/GAG-PA treated groups relative to autograft and K-PA/E-PA treated groups. This result indicates that biologically active LN-PA/GAG-PA can be used clinically in hollow polymeric tubes without any negative effects on the overall morphology for the peripheral nerve injury treatment.

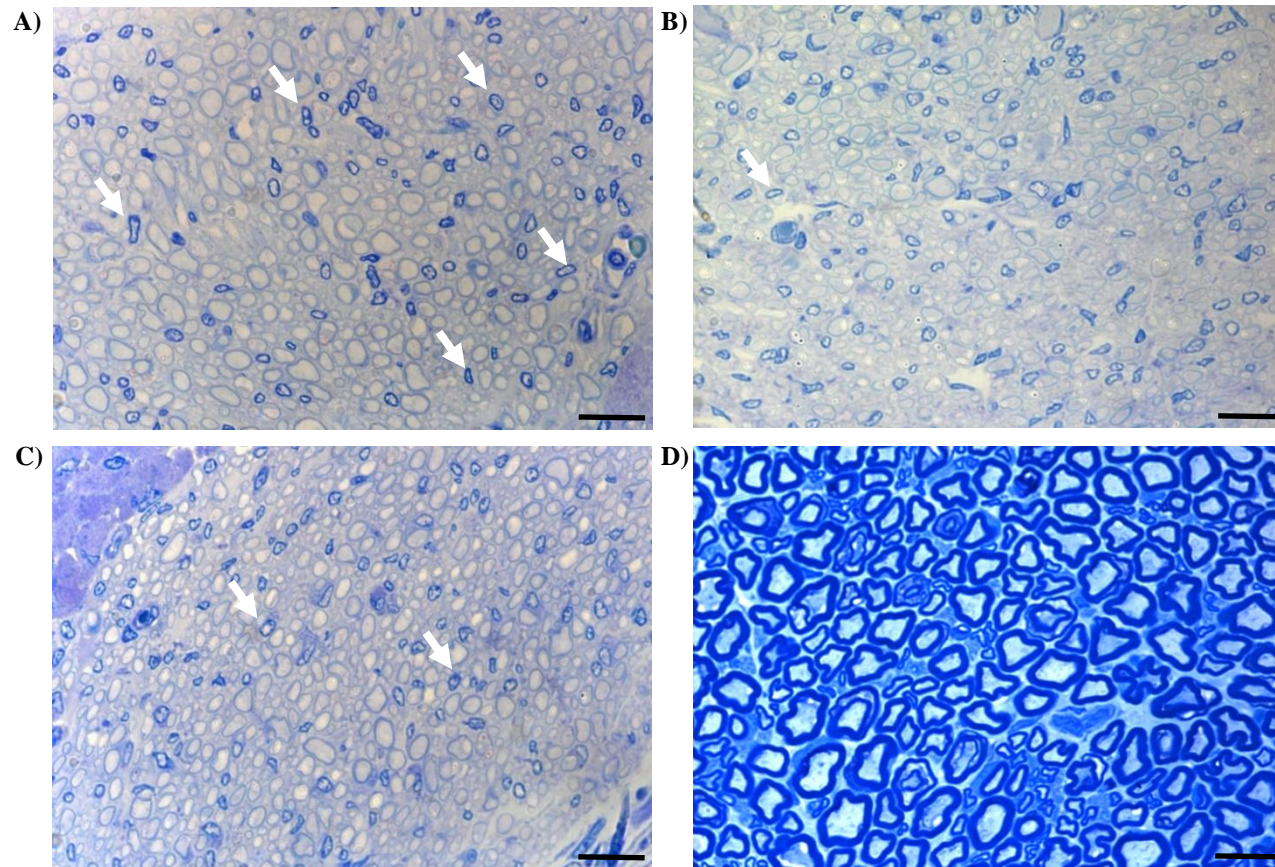


**Figure 2.14.** Toluidine Blue-O stained semi-thin transverse sections of resin embedded tissues. Schwann cells are indicated with white arrows. LN-PA/GAG-PA (**A-C**), Healthy (**D**) groups. Scale bars are 100  $\mu\text{m}$ .

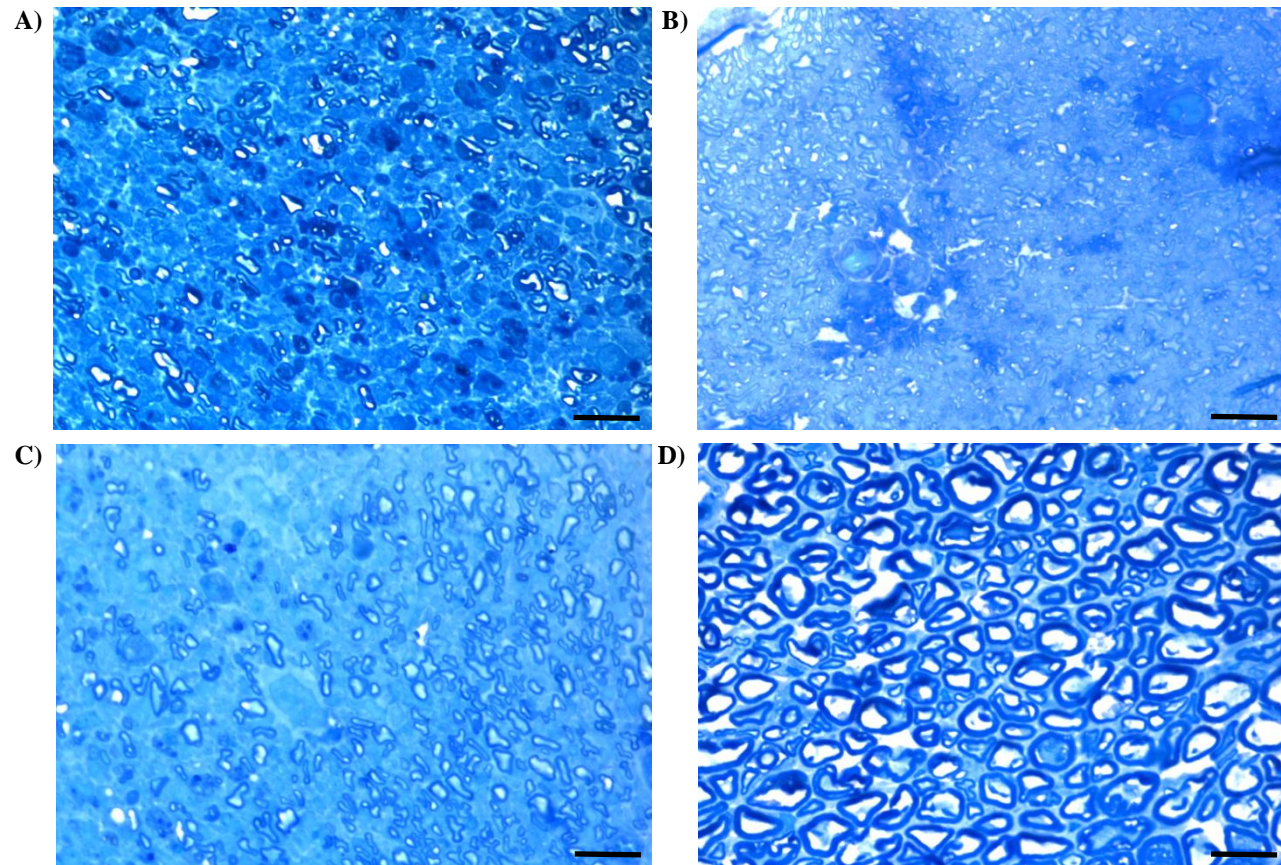


**Figure 2.15.** Toluidine Blue-O stained semi-thin transverse sections of resin embedded tissues. K-PA/E-PA (A-C), Healthy (D) groups.

Scale bars are 100  $\mu\text{m}$ .

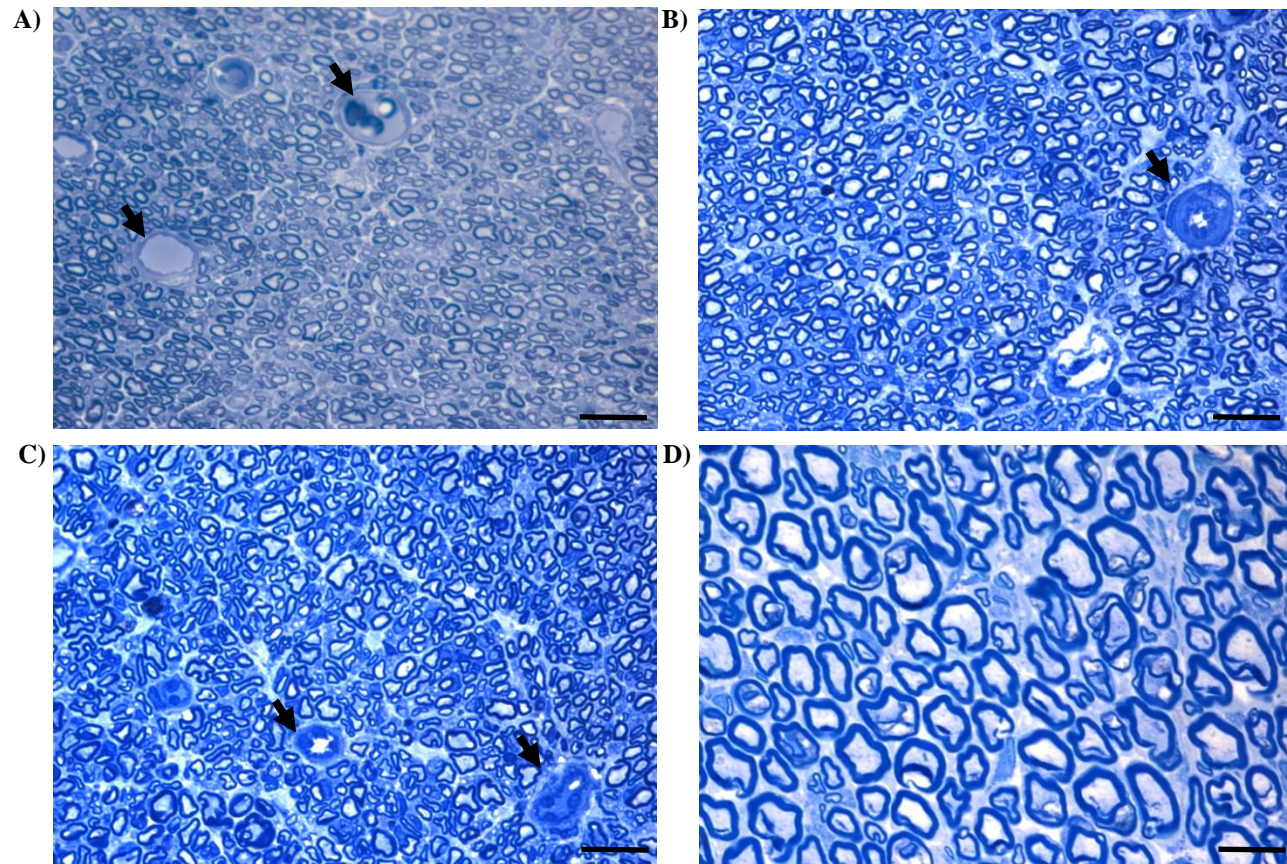


**Figure 2.16.** Toluidine Blue-O stained semi-thin transverse sections of resin embedded tissues. Undefined morphological structures are indicated with black arrows. Sucrose (A-C), Healthy (D) groups. Scale bars are 100  $\mu\text{m}$ .

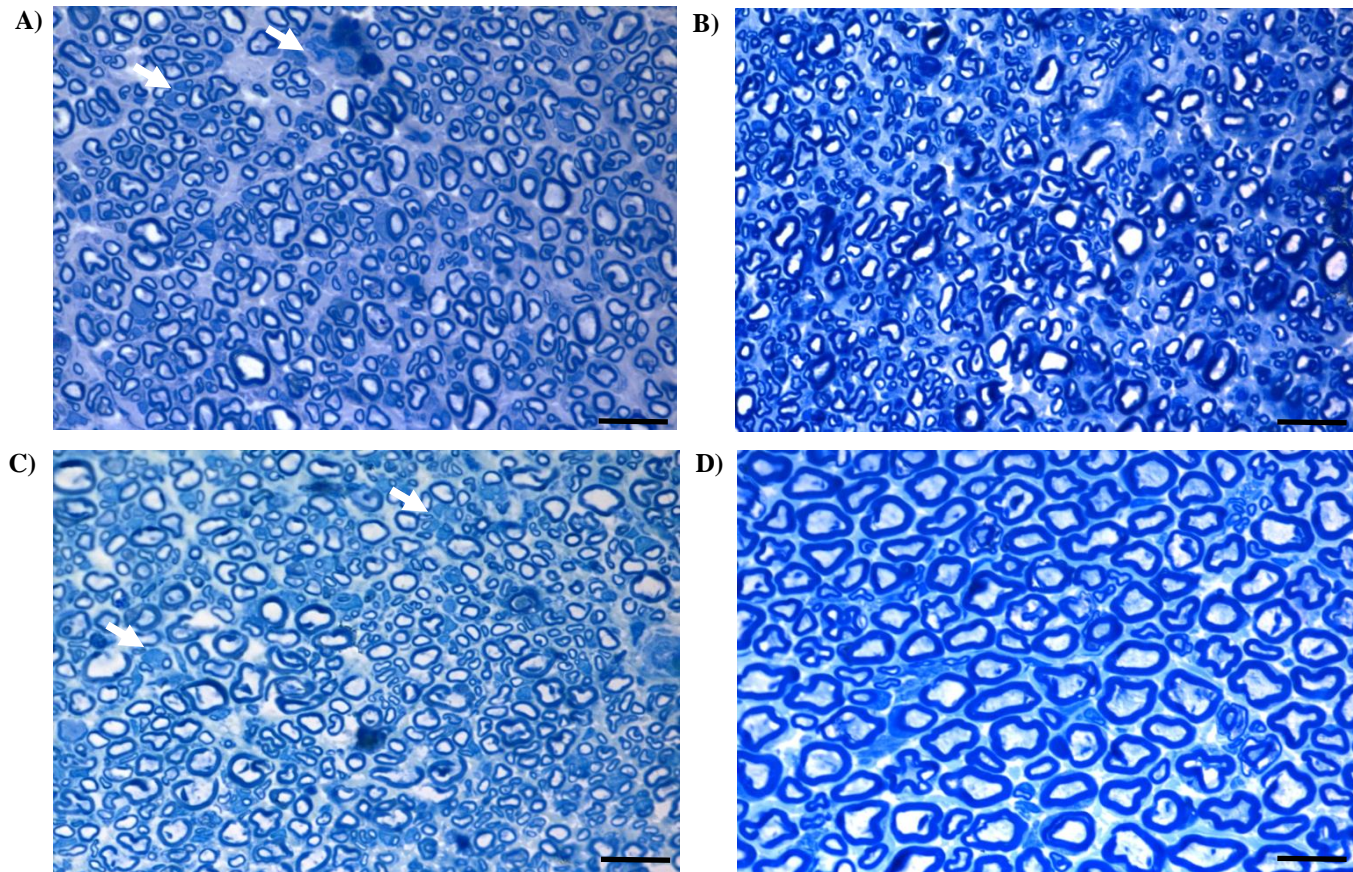


**Figure 2.17.** Toluidine Blue-O stained semi-thin transverse sections of resin embedded tissues. Several stages of degeneration are indicated with white arrows. Autograft (A-C), Healthy (D) groups. Scale bars are 100  $\mu\text{m}$

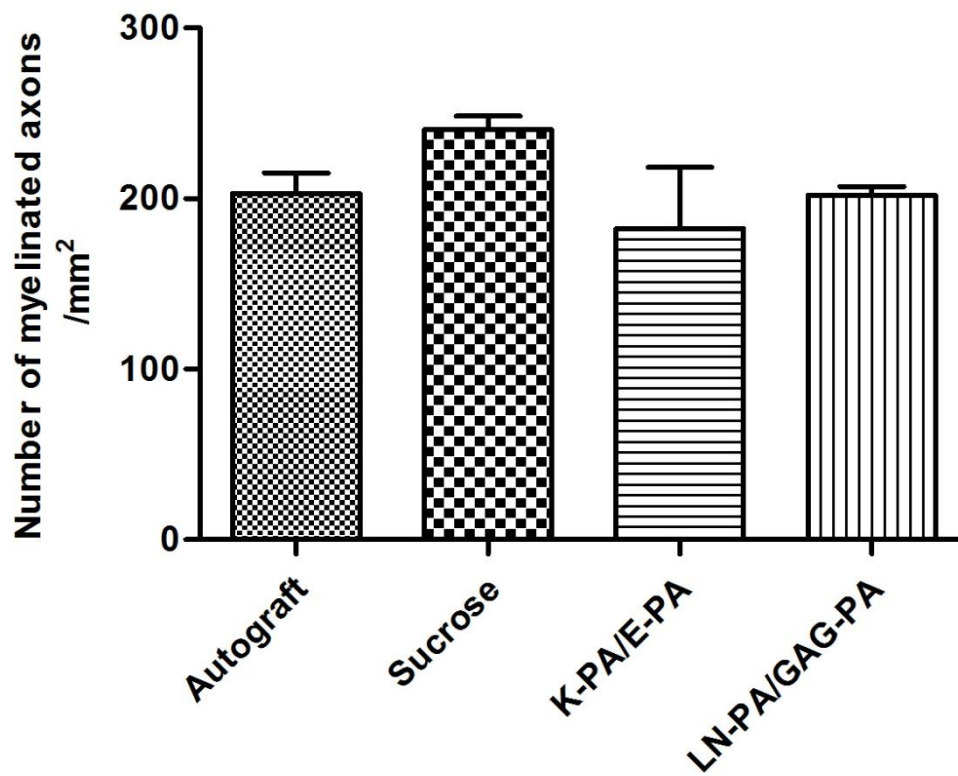


**Figure 2.18.** Quantification of the number of myelinated axons/mm<sup>2</sup> from semi-thin sectioned sciatic nerve tissues stained with toluidine blue-O. Statistical analysis was performed with GraphPad Prism 5.01 applying One-way ANOVA.

Axonal regeneration was also investigated by transverse ultrathin sections from the mid-part of excised sciatic nerve tissue. Ultrastructural morphologies of all treatment groups and healthy nerve tissues were observed under transmission and scanning transmission electron microscope (Figure 2.19-23). General morphological trends were in good correlation with toluidine blue-O staining of all treatment groups. The most similar ultrastructural morphology to healthy nerve tissue structure was seen in LN-PA/GAG-PA treated groups which was also seen in toluidine blue-O staining (Figure 2.19). Moreover, abnormal fiber morphology was seen in K-PA/E-PA treated groups, as well as in toluidine blue staining. Several stages of axonal injury and its progression to abnormal morphology during myelination and demyelination of degenerated fibers can be clearly seen, especially for autograft groups under examination on the basis of contemporary peripheral nerve histopathology. The morphological examination of autograft treatment group revealed that Schwann cells were surrounded with onion-bulb like structures which are characteristic signs of demyelination and axonal degeneration (white arrows) (Figure 2.17). Swollen axons were clearly observed in empty conduit treated groups.

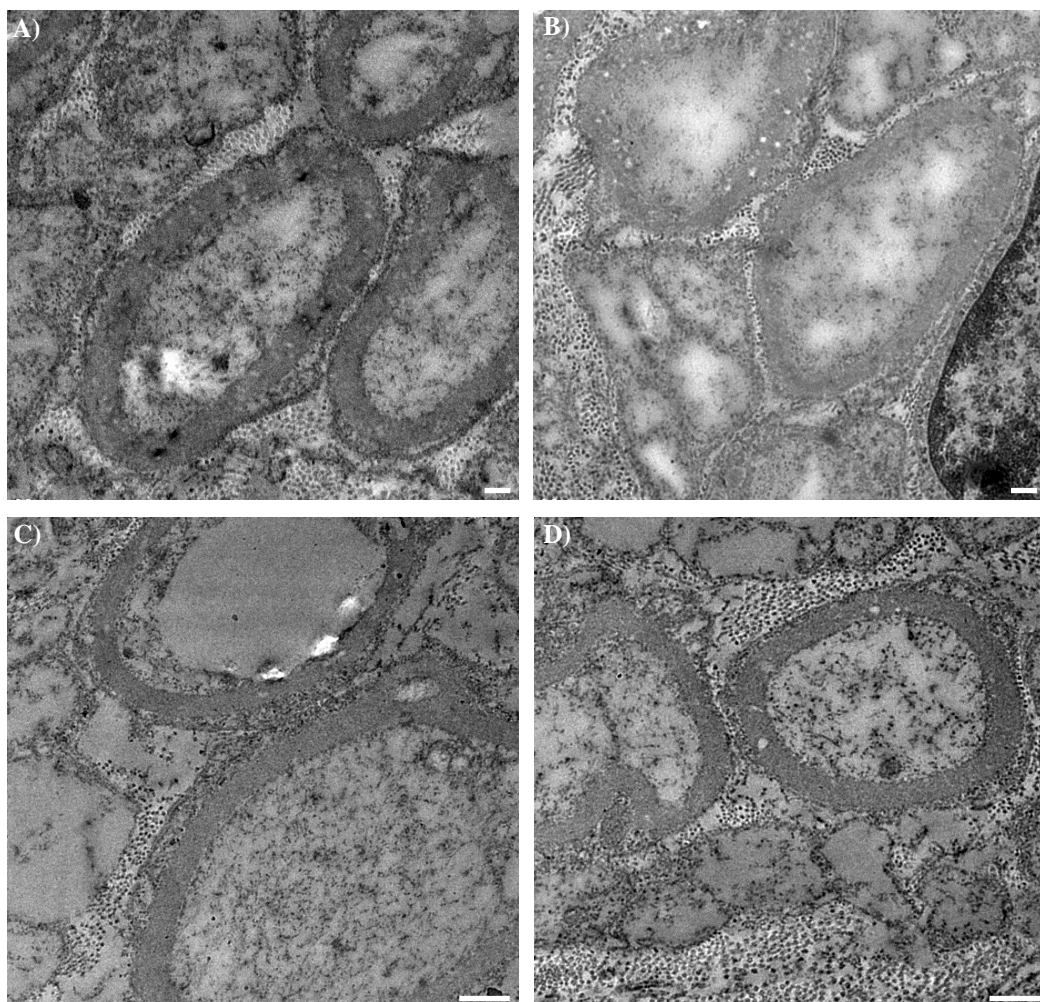


**Figure 2.19.** Transmission electron micrograph (TEM) of LN-PA/GAG-PA filled conduit treated group. Scale bars are 200 nm (A) and 500 nm (B-D).

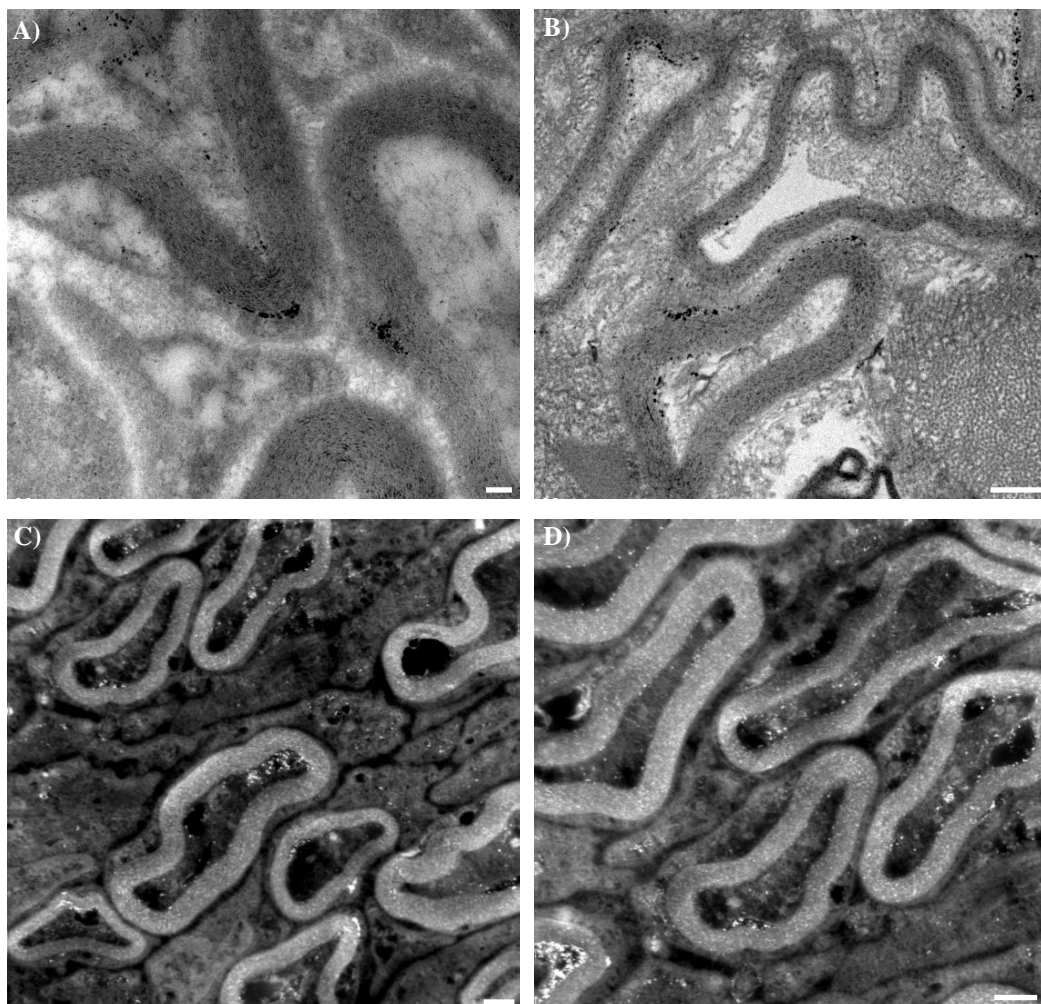


**Figure 2.20.** Transmission electron micrograph (TEM) of K-PA/E-PA filled conduit treated group (A, B) and scanning transmission electron micrograph (STEM) of K-PA/E-PA filled conduit treated group (C, D). Scale bars are 200 nm (A) and 500 nm (B-D).

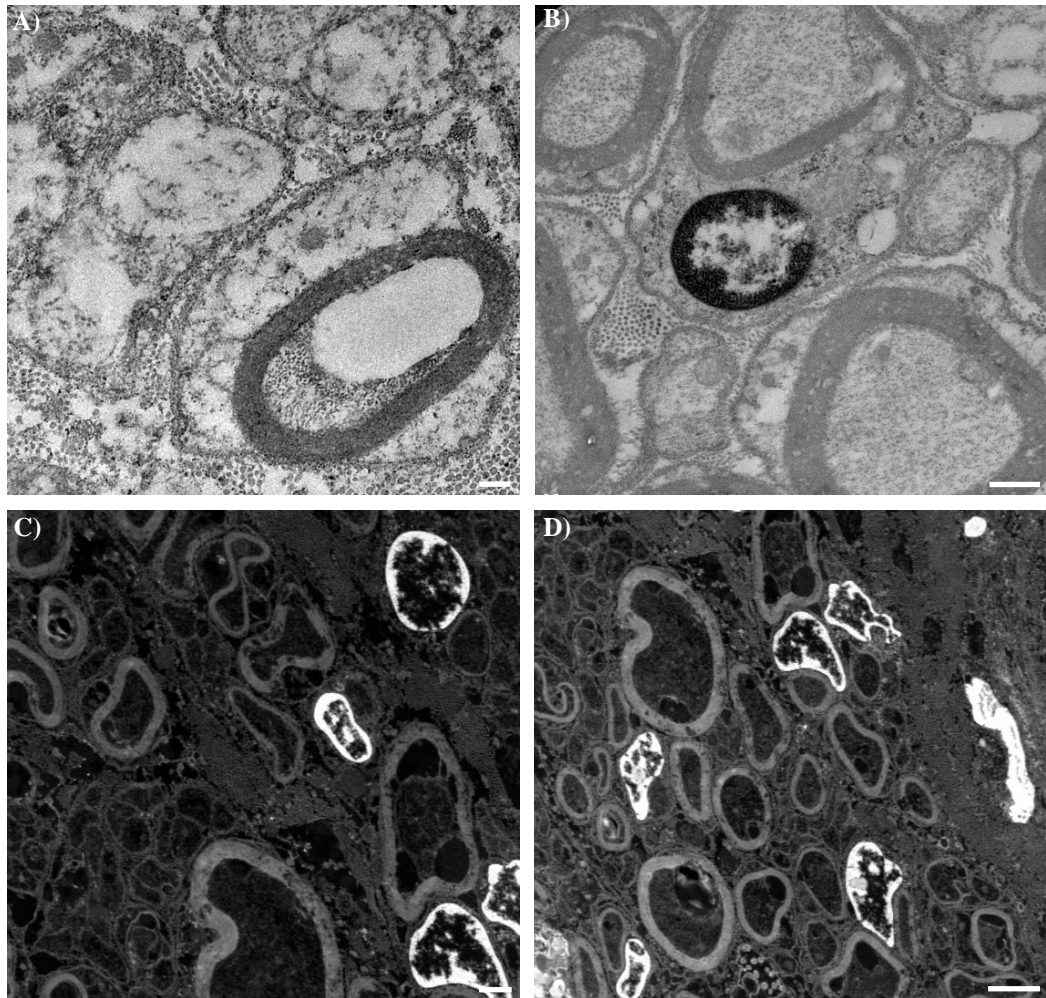


**Figure 2.21.** Transmission electron micrograph (TEM) of sucrose filled conduit treated group (**A, B**) and scanning transmission electron micrograph (STEM) of sucrose filled conduit treated group (**C, D**). Scale bars are 200 nm (**A**), 500 nm (**B, C**) and 2  $\mu$ m (**D**).

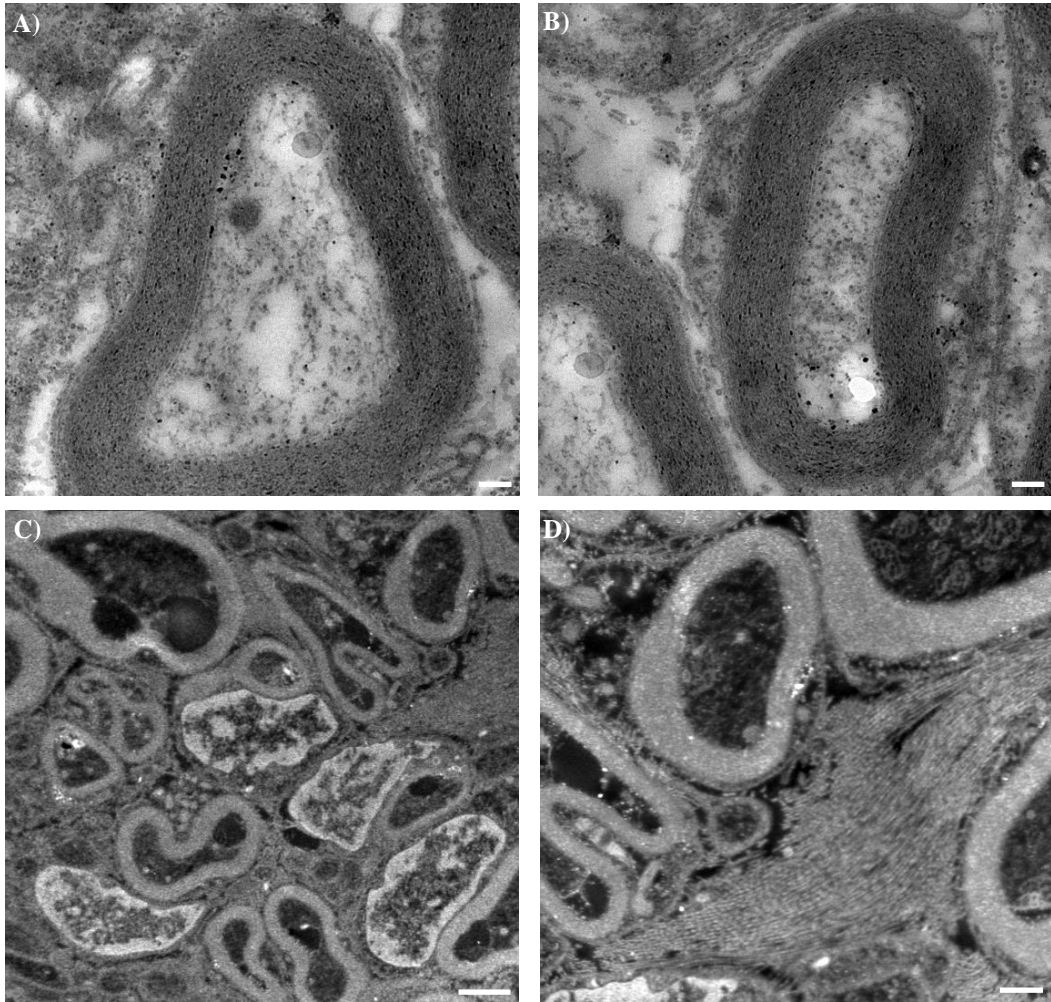


**Figure 2.22.** Transmission electron micrograph (TEM) of autograft treated group (**A**, **B**) and scanning transmission electron micrograph (STEM) of autograft treated group (**C**, **D**). Scale bars are 200 nm (**A**, **B**), 500 nm (**D**) and 2  $\mu$ m (**C**).

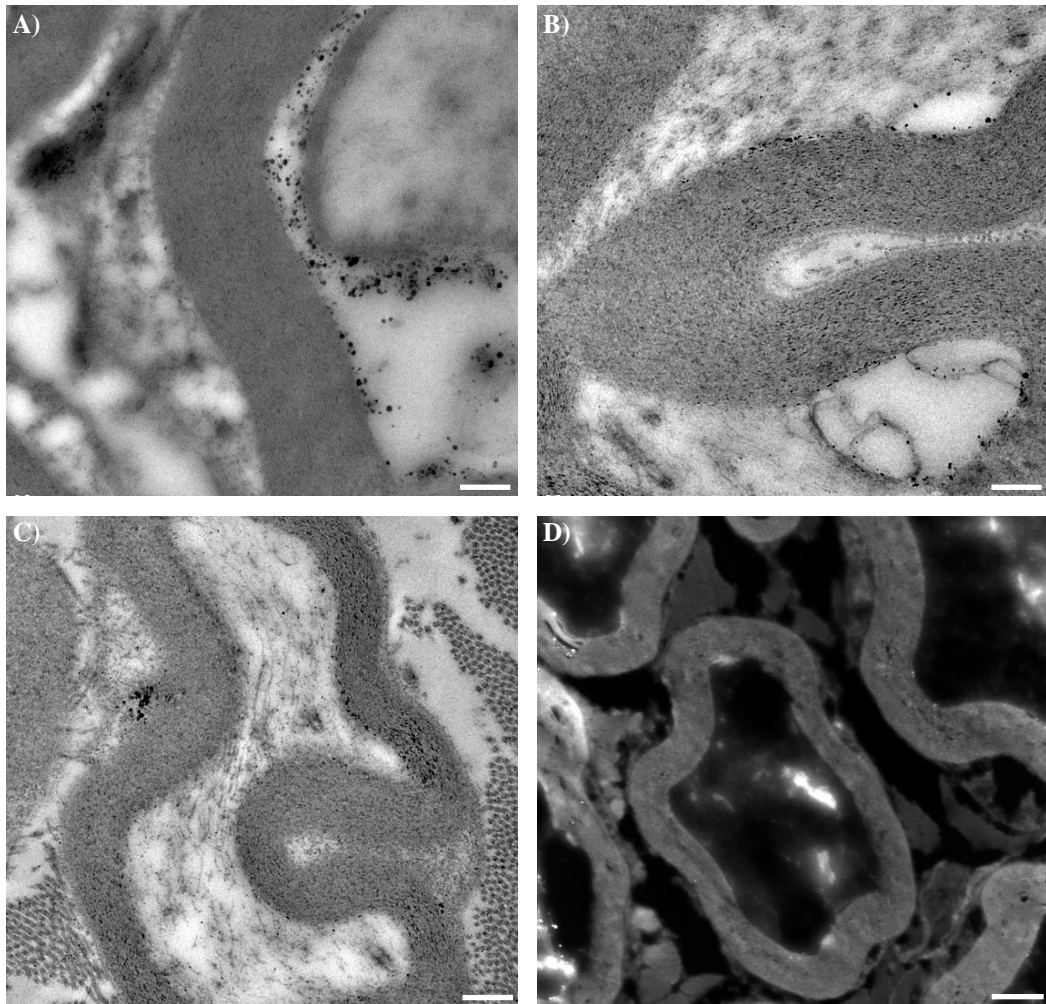


**Figure 2.23.** Transmission electron micrograph (TEM) of healthy group (A-C) and scanning transmission electron micrograph (STEM) of healthy group (D). Scale bars are 500 nm (A-C) and 2  $\mu\text{m}$  (D).

The quantitative analysis showed that the axonal diameter of the myelinated fibers was larger in LN-PA/GAG-PA treated group when compared to sucrose and K-PA/E-PA groups (Figure 2.24). Autograft treated group had the largest axonal diameter owing to the presence of Schwann cells that secrete growth factors [14] and laminin [75], and produce the myelin sheath, but sucrose treated group had the thinnest axonal diameter.

12 weeks after injury, quantitative analysis of myelination thickness showed that the thickness of well-myelinated axons in the regenerating nerve was higher in LN-PA/GAG-PA filled conduit group relative to both sucrose and K-PA/E-PA filled conduit groups. In addition, the myelination thickness in the K-PA/E-PA treated group was the thinnest (Figure 2.25). In autograft group, newborn axons were encountered less frequently when compared to other treatment groups. Therefore, because of the presence of Schwann cells and basal lamina of endoneurial tube in autograft nerve tissue, the thickness of myelin sheath was the highest relative to the other treatment groups.

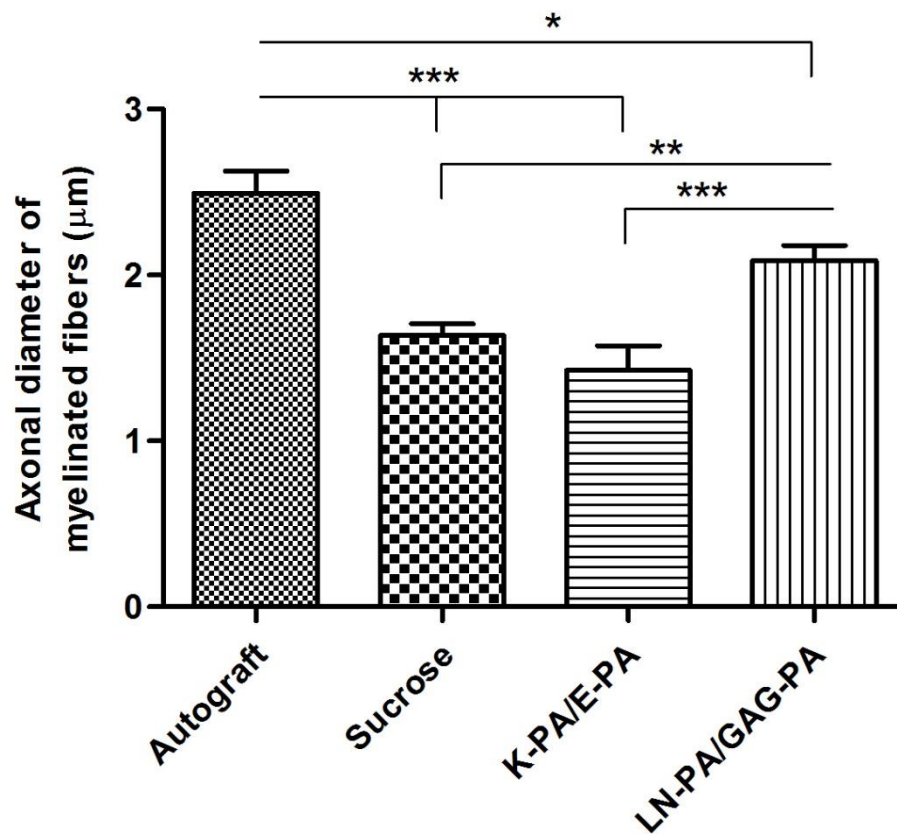


**Figure 2.24.** Quantification of axonal diameter of myelinated fibers on ultrathin transverse sections. Statistical analysis was performed with GraphPad Prism 5.01 applying One-way ANOVA ( $p < 0.05$  (\*),  $p < 0.01$  (\*\*),  $p < 0.001$  (\*\*\*)).

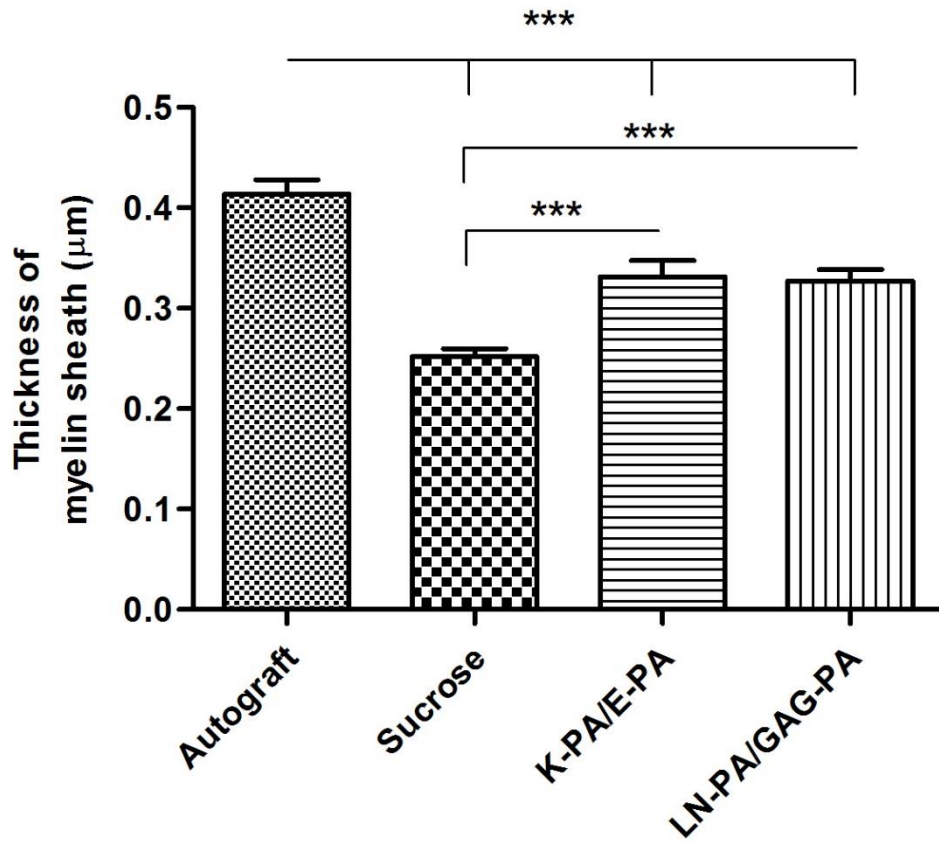


**Figure 2.25.** Myelination thickness quantification of ultrathin transverse sections. Statistical analysis was performed with GraphPad Prism 5.01 applying One-way ANOVA ( $p < 0.001$  (\*\*\*)).

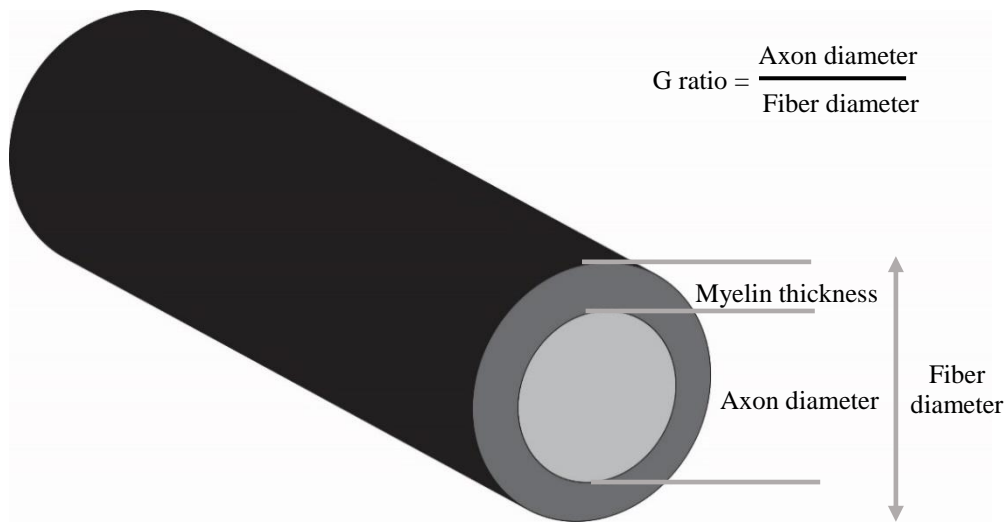


**Figure 2.26.** Representative diagram indicating the critical nerve tissue fiber parameters.

Myelination is an important cellular process that can cause a noticeable effect on the morphological characteristic structure and physiology of an axon and its surrounding tissue. It is generally affirmed view that the ratio of axonal diameter to the total fiber diameter known as the g ratio is important to evaluate axonal myelination (Figure 2.26). Moreover, the measurement of g ratio of myelinated axons is optimized for the restoration of damaged nerve tissue to reach the maximal efficiency and physiological optimization [147-149]. In the literature, g ratio value for myelinate axons was optimized and this ratio is 0.55-0.68 for sciatic nerve [150-153]. According to the quantification results, LN-PA/GAG-PA treated group and sucrose treated group have the highest g ratio relative to the other groups. However, there is no significant

difference between LN-PA/GAG-PA and sucrose group. The g ratio value is higher than 0.7 except K-PA/E-PA treated group (Figure 2.27).

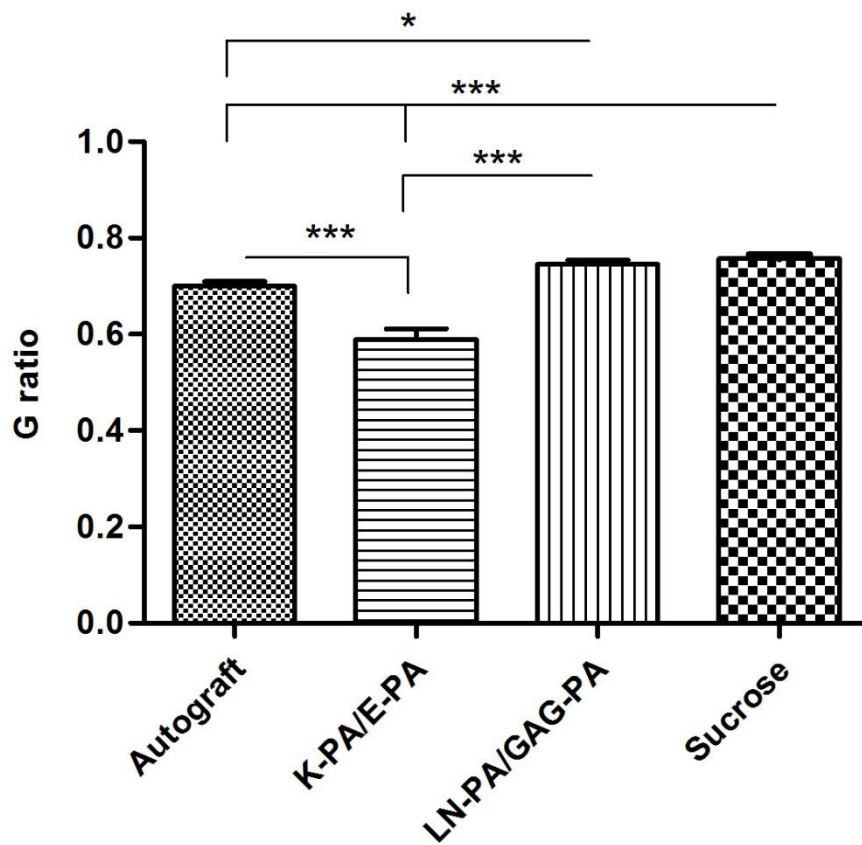


**Figure 2.27.** G ratio quantification of ultrathin transverse sections. Statistical analysis was performed with GraphPad Prism 5.01 applying One-way ANOVA ( $p < 0.05$  (\*),  $p < 0.01$  (\*\*),  $p < 0.001$  (\*\*\*)).

# **CHAPTER 3**

## **CONCLUSION AND FUTURE PERSPECTIVES**

Deeply understanding of tissue and organ hierarchy and response of cell-cell signaling and cell-material interaction will give tips to design novel biomaterials and scaffolds for tissue engineering and regenerative medicine. Moreover, investigation and comprehension of the parameters for modulating cell fate and microenvironment will affect the methodology of scaffold design. This combinatorial approach have affected life quality and expectancy of people that suffer from neurodegenerative disorders, physical traumas and nerve injuries resulting in loss of motor and sensory functions, neuropathic pain and organ atrophy. Nervous system has a highly complex tissue structure and the limitations including lack of proliferation capacity, and inhibitory environment occurring after injury is really challenging. Conventional surgical intervention including end to end coaptation is a treatment option when nerve gap is shorter than 1 cm. Longer nerve gaps, which are prevalent after more serious injuries, are generally treated with autologous nerve grafting, cadaveric nerve transplantation or nerve conduits.

In this thesis, I used histological analyses and TEM imaging to analyze the effect of self-assembled peptide nanofiber platforms designed as extracellular matrix mimetic scaffolds to lead successful neural regeneration. These peptide amphiphile molecules can self-assemble into nanofiber scaffolds due to their hydrophobic core and hydrophilic surface. Bioactive signals inspired from the ECM of nerve cells can be presented by peptide nanofibers. In this study, laminin-mimetic and heparan sulfate-mimetic PA molecules were used. Laminin-mimetic PA molecule, LN-PA, is indispensable for Schwann cell proliferation, migration and myelination process. Another peptide molecule, GAG-PA, mimics glycosylated heparan sulfate molecules,

which are also found in the basal lamina of peripheral nerves. Neuroinductive growth factors especially bFGF and NGF can bind to HS and avoid proteolysis. The neuroinductive effect of both LN-PA/GAG-PA gel system and autologous nerve grafting was evaluated by using full transection rat sciatic nerve model. *Neurolac*<sup>®</sup> TW was used as a polymeric guidance channel and filled with LN-PA/GAG-PA nanofiber gels for biofunctionalization of hollow tubes. Empty NGCs filled with sucrose and epitope free peptide nanofiber gels were used as control groups. 12 weeks after operation, electrophysiological assessment was performed and EMG results showed that signal transmission was better in LN-PA/GAG-PA treated nerves relative to other treatment groups. Histological examinations revealed that good linearity, and better axonal regeneration at the both proximal and distal site of truncated nerve were seen in LN-PA/GAG-PA functionalized conduits. Insufficient innervation and swollen axon morphologies were seen in autograft and epitope free peptide nanofiber treated groups. According to the quantitative analysis of TEM and STEM images, LN-PA/GAG-PA had the higher axonal diameter and myelin thickness relative to the sucrose and K-PA/E-PA treated groups except autograft because of the presence of Schwann cells. Schwann cells secrete growth factors, produce myelin sheath and induce production of laminin. Currently, in cable autograft technique used in the clinic, many nonfunctioning small-caliber nerves aligned in parallel to span a nerve gap, but in this study we used entire sciatic nerve graft for autograft group. Therefore, these results showed that this bioactive gel system inserted into *Neurolac*<sup>®</sup> TW conduits may be used clinically without any negative effects on peripheral nerve regeneration. For further studies, genetically modified cells or pluripotent stem cells within biologically engineered conduits can be used for successful peripheral nerve regeneration. In order

to provide better recovery after injuries, neurogenic growth factors or small molecules having analgesic properties that can be encapsulated into both polymeric neural tubes and hydrogels.

## BIBLIOGRAPHY

1. Noble, J., et al., *Analysis of upper and lower extremity peripheral nerve injuries in a population of patients with multiple injuries*. Journal of Trauma and Acute Care Surgery, 1998. **45**(1): p. 116-122.
2. Mumenthaler, M., M. Stöhr, and H. Müller-Vahl, *Läsionen peripherer Nerven und radikuläre Syndrome*. 2007: Georg Thieme Verlag.
3. Nicholson, B. and S. Verma, *Comorbidities in chronic neuropathic pain*. Pain medicine, 2004. **5**(s1): p. S9-S27.
4. Taylor, R.S., *Epidemiology of refractory neuropathic pain*. Pain Practice, 2006. **6**(1): p. 22-26.
5. Schlosshauer, B., et al., *Synthetic nerve guide implants in humans: a comprehensive survey*. Neurosurgery, 2006. **59**(4): p. 740-748.
6. Sunderland, S., *A classification of peripheral nerve injuries producing loss of function*. Brain, 1951. **74**(4): p. 491-516.
7. Lundborg, G., *A 25-year perspective of peripheral nerve surgery: evolving neuroscientific concepts and clinical significance*. The Journal of hand surgery, 2000. **25**(3): p. 391-414.
8. David, S. and A.J. Aguayo, *Axonal elongation into peripheral nervous system "bridges" after central nervous system injury in adult rats*. Science, 1981. **214**(4523): p. 931-933.
9. Richardson, P., U. McGuinness, and A. Aguayo, *Axons from CNS neurones regenerate into PNS grafts*. 1980.
10. Varon, S.S. and R.P. Bunge, *Trophic mechanisms in the peripheral nervous system*. Annual review of neuroscience, 1978. **1**(1): p. 327-361.

11. Yan, Q., J. Elliott, and W.D. Snider, *Brain-derived neurotrophic factor rescues spinal motor neurons from axotomy-induced cell death*. *Nature*, 1992. **360**(6406): p. 753-755.
12. Yin, Q., G. Kemp, and S. Frostick, *Neurotrophins, neurones and peripheral nerve regeneration*. *Journal of Hand Surgery (British and European Volume)*, 1998. **23**(4): p. 433-437.
13. Cavanaugh, M.W., *Quantitative effects of the peripheral innervation area on nerves and spinal ganglion cells*. *Journal of Comparative Neurology*, 1951. **94**(2): p. 181-219.
14. Chen, Z.-L., W.-M. Yu, and S. Strickland, *Peripheral regeneration*. *Annu. Rev. Neurosci.*, 2007. **30**: p. 209-233.
15. Patton, B.L., et al., *Distribution and function of laminins in the neuromuscular system of developing, adult, and mutant mice*. *The Journal of cell biology*, 1997. **139**(6): p. 1507-1521.
16. Bourde, O., et al., *Quantification of interleukin-6 mRNA in wallerian degeneration by competitive reverse transcription polymerase chain reaction*. *Journal of neuroimmunology*, 1996. **69**(1): p. 135-140.
17. Banner, L.R. and P.H. Patterson, *Major changes in the expression of the mRNAs for cholinergic differentiation factor/leukemia inhibitory factor and its receptor after injury to adult peripheral nerves and ganglia*. *Proceedings of the National Academy of Sciences*, 1994. **91**(15): p. 7109-7113.
18. Heumann, R., et al., *Differential regulation of mRNA encoding nerve growth factor and its receptor in rat sciatic nerve during development, degeneration, and regeneration: role of macrophages*. *Proceedings of the National Academy of Sciences*, 1987. **84**(23): p. 8735-8739.

19. Markus, A., T.D. Patel, and W.D. Snider, *Neurotrophic factors and axonal growth*. *Current opinion in neurobiology*, 2002. **12**(5): p. 523-531.
20. Snider, W.D., et al., *Signaling the pathway to regeneration*. *Neuron*, 2002. **35**(1): p. 13-16.
21. Fu, S.Y. and T. Gordon, *The cellular and molecular basis of peripheral nerve regeneration*. *Molecular neurobiology*, 1997. **14**(1-2): p. 67-116.
22. Scott, A.L. and M.S. Ramer, *Schwann cell p75<sup>NTR</sup> prevents spontaneous sensory reinnervation of the adult spinal cord*. *Brain*, 2010. **133**(2): p. 421-432.
23. Perry, V., M. Brown, and S. Gordon, *The macrophage response to central and peripheral nerve injury. A possible role for macrophages in regeneration*. *The Journal of experimental medicine*, 1987. **165**(4): p. 1218-1223.
24. Ann, E.S., et al., *Motor axon terminal regeneration as studied by protein gene product 9.5 immunohistochemistry in the rat*. *Archives of histology and cytology*, 1994. **57**(4): p. 317-330.
25. Son, Y.-J. and W.J. Thompson, *Schwann cell processes guide regeneration of peripheral axons*. *Neuron*, 1995. **14**(1): p. 125-132.
26. Wall, P., et al., *Autotomy following peripheral nerve lesions: experimental anesthesia dolorosa*. *Pain*, 1979. **7**(2): p. 103-113.
27. Jiang, X., et al., *Current applications and future perspectives of artificial nerve conduits*. *Experimental neurology*, 2010. **223**(1): p. 86-101.
28. Madduri, S., M. Papaloizos, and B. Gander, *Trophically and topographically functionalized silk fibroin nerve conduits for guided peripheral nerve regeneration*. *Biomaterials*, 2010. **31**(8): p. 2323-2334.

29. Siemionow, M., M. Bozkurt, and F. Zor, *Regeneration and repair of peripheral nerves with different biomaterials: review*. *Microsurgery*, 2010. **30**(7): p. 574-588.
30. Belkas, J.S., M.S. Shoichet, and R. Midha, *Peripheral nerve regeneration through guidance tubes*. *Neurological research*, 2004. **26**(2): p. 151-160.
31. Johnson, E.O. and P.N. Soucacos, *Nerve repair: experimental and clinical evaluation of biodegradable artificial nerve guides*. *Injury*, 2008. **39**(3): p. 30-36.
32. Lee, S.K. and S.W. Wolfe, *Peripheral nerve injury and repair*. *Journal of the American Academy of Orthopaedic Surgeons*, 2000. **8**(4): p. 243-252.
33. Pabari, A., et al., *Modern surgical management of peripheral nerve gap*. *Journal of Plastic, Reconstructive & Aesthetic Surgery*, 2010. **63**(12): p. 1941-1948.
34. Evans, G.R., *Peripheral nerve injury: a review and approach to tissue engineered constructs*. *The Anatomical Record*, 2001. **263**(4): p. 396-404.
35. Bellamkonda, R.V., *Peripheral nerve regeneration: an opinion on channels, scaffolds and anisotropy*. *Biomaterials*, 2006. **27**(19): p. 3515-3518.
36. Chen, M.B., F. Zhang, and W.C. Lineaweaver, *Luminal fillers in nerve conduits for peripheral nerve repair*. *Annals of plastic surgery*, 2006. **57**(4): p. 462-471.
37. Panseri, S., et al., *Electrospun micro-and nanofiber tubes for functional nervous regeneration in sciatic nerve transections*. *Bmc Biotechnology*, 2008. **8**(1): p. 39.

38. Siemionow, M. and G. Brzezicki, *Current techniques and concepts in peripheral nerve repair*. International review of neurobiology, 2009. **87**: p. 141-172.
39. Moradzadeh, A., et al., *The impact of motor and sensory nerve architecture on nerve regeneration*. Experimental neurology, 2008. **212**(2): p. 370-376.
40. Ijpma, F., R. Van De Graaf, and M. Meek, *The early history of tubulation in nerve repair*. Journal of Hand Surgery (European Volume), 2008. **33**(5): p. 581-586.
41. de Ruitter, G.C., et al., *Designing ideal conduits for peripheral nerve repair*. Neurosurgical focus, 2009. **26**(2): p. E5.
42. Griffin, J., et al., *Design and evaluation of novel polyanhydride blends as nerve guidance conduits*. Acta biomaterialia, 2010. **6**(6): p. 1917-1924.
43. Chiono, V., C. Tonda-Turo, and G. Ciardelli, *Artificial scaffolds for peripheral nerve reconstruction*. International review of neurobiology, 2009. **87**: p. 173-198.
44. Chalfoun, C., G. Wirth, and G. Evans, *Tissue engineered nerve constructs: where do we stand?* Journal of cellular and molecular medicine, 2006. **10**(2): p. 309-317.
45. Hudson, T.W., G.R. Evans, and C.E. Schmidt, *Engineering strategies for peripheral nerve repair*. Orthopedic Clinics, 2000. **31**(3): p. 485-497.
46. Subramanian, A., U.M. Krishnan, and S. Sethuraman, *Development of biomaterial scaffold for nerve tissue engineering: Biomaterial mediated neural regeneration*. J Biomed Sci, 2009. **16**(1): p. 108.

47. Ahmed, I., et al., *Three-dimensional nanofibrillar surfaces covalently modified with tenascin-C-derived peptides enhance neuronal growth in vitro*. Journal of Biomedical Materials Research Part A, 2006. **76**(4): p. 851-860.
48. Okamoto, H., et al., *Recovery process of sciatic nerve defect with novel bioabsorbable collagen tubes packed with collagen filaments in dogs*. Journal of Biomedical Materials Research Part A, 2010. **92**(3): p. 859-868.
49. Corey, J.M., et al., *Aligned electrospun nanofibers specify the direction of dorsal root ganglia neurite growth*. Journal of Biomedical Materials Research Part A, 2007. **83**(3): p. 636-645.
50. Patel, S., et al., *Bioactive nanofibers: synergistic effects of nanotopography and chemical signaling on cell guidance*. Nano letters, 2007. **7**(7): p. 2122-2128.
51. Chew, S.Y., et al., *The effect of the alignment of electrospun fibrous scaffolds on Schwann cell maturation*. Biomaterials, 2008. **29**(6): p. 653-661.
52. Chew, S.Y., et al., *Sustained release of proteins from electrospun biodegradable fibers*. Biomacromolecules, 2005. **6**(4): p. 2017-2024.
53. Wang, S., et al., *Photo-crosslinked poly ( $\epsilon$ -caprolactone fumarate) networks for guided peripheral nerve regeneration: Material properties and preliminary biological evaluations*. Acta biomaterialia, 2009. **5**(5): p. 1531-1542.
54. Kim, I.A., et al., *Effects of mechanical stimuli and microfiber-based substrate on neurite outgrowth and guidance*. Journal of bioscience and bioengineering, 2006. **101**(2): p. 120-126.
55. Nisbet, D., et al., *Interaction of embryonic cortical neurons on nanofibrous scaffolds for neural tissue engineering*. Journal of Neural Engineering, 2007. **4**(2): p. 35.

56. Chow, W.N., et al., *Evaluating neuronal and glial growth on electrospun polarized matrices: bridging the gap in percussive spinal cord injuries*. *Neuron glia biology*, 2007. **3**(02): p. 119-126.
57. Cao, J., et al., *The use of laminin modified linear ordered collagen scaffolds loaded with laminin-binding ciliary neurotrophic factor for sciatic nerve regeneration in rats*. *Biomaterials*, 2011. **32**(16): p. 3939-3948.
58. Neal, R.A., et al., *Laminin nanofiber meshes that mimic morphological properties and bioactivity of basement membranes*. *Tissue Engineering Part C: Methods*, 2008. **15**(1): p. 11-21.
59. Wang, W., et al., *Influences of mechanical properties and permeability on chitosan nano/microfiber mesh tubes as a scaffold for nerve regeneration*. *Journal of Biomedical Materials Research Part A*, 2008. **84**(2): p. 557-566.
60. Dodla, M.C. and R.V. Bellamkonda, *Differences between the effect of anisotropic and isotropic laminin and nerve growth factor presenting scaffolds on nerve regeneration across long peripheral nerve gaps*. *Biomaterials*, 2008. **29**(1): p. 33-46.
61. Midha, R., et al., *Growth factor enhancement of peripheral nerve regeneration through a novel synthetic hydrogel tube*. *Journal of neurosurgery*, 2003. **99**(3): p. 555-565.
62. Xu, X.M., et al., *Bridging Schwann cell transplants promote axonal regeneration from both the rostral and caudal stumps of transected adult rat spinal cord*. *Journal of neurocytology*, 1997. **26**(1): p. 1-16.
63. Zahir, T., et al., *Bioengineering neural stem/progenitor cell-coated tubes for spinal cord injury repair*. *Cell transplantation*, 2008. **17**(3): p. 245-254.

64. Meek, M.F., J. Nicolai, and P.H. Robinson, *Secondary digital nerve repair in the foot with resorbable p (DLLA-epsilon-CL) nerve conduits*. Journal of reconstructive microsurgery, 2006. **22**(3): p. 149-151.
65. Kehoe, S., X. Zhang, and D. Boyd, *FDA approved guidance conduits and wraps for peripheral nerve injury: a review of materials and efficacy*. Injury, 2012. **43**(5): p. 553-572.
66. Reichardt, L.F. and K.J. Tomaselli, *Extracellular matrix molecules and their receptors: functions in neural development*. Annual review of neuroscience, 1991. **14**: p. 531.
67. Makwana, M. and G. Raivich, *Molecular mechanisms in successful peripheral regeneration*. Febs Journal, 2005. **272**(11): p. 2628-2638.
68. Richardson, P. and V. Issa, *Peripheral injury enhances central regeneration of primary sensory neurones*. 1984.
69. Neumann, S., et al., *Regeneration of sensory axons within the injured spinal cord induced by intraganglionic cAMP elevation*. Neuron, 2002. **34**(6): p. 885-893.
70. Qiu, J., et al., *Spinal axon regeneration induced by elevation of cyclic AMP*. Neuron, 2002. **34**(6): p. 895-903.
71. Qiu, J., D. Cai, and M.T. Filbin, *A role for cAMP in regeneration during development and after injury*. Progress in brain research, 2002. **137**: p. 381.
72. Cai, D., et al., *Arginase I and polyamines act downstream from cyclic AMP in overcoming inhibition of axonal growth MAG and myelin in vitro*. Neuron, 2002. **35**(4): p. 711-719.

73. Gao, Y., et al., *Activated CREB is sufficient to overcome inhibitors in myelin and promote spinal axon regeneration in vivo*. *Neuron*, 2004. **44**(4): p. 609-621.
74. Raivich, G., et al., *The AP-1 transcription factor c-Jun is required for efficient axonal regeneration*. *Neuron*, 2004. **43**(1): p. 57-67.
75. Luckenbill-Edds, L., *Laminin and the mechanism of neuronal outgrowth*. *Brain Research Reviews*, 1997. **23**(1): p. 1-27.
76. Martini, R., *Expression and functional roles of neural cell surface molecules and extracellular matrix components during development and regeneration of peripheral nerves*. *Journal of neurocytology*, 1994. **23**(1): p. 1-28.
77. Chen, Z.-L. and S. Strickland, *Laminin  $\gamma 1$  is critical for Schwann cell differentiation, axon myelination, and regeneration in the peripheral nerve*. *The Journal of cell biology*, 2003. **163**(4): p. 889-899.
78. Tashiro, K.-i., et al., *A synthetic peptide containing the IKVAV sequence from the A chain of laminin mediates cell attachment, migration, and neurite outgrowth*. *Journal of Biological Chemistry*, 1989. **264**(27): p. 16174-16182.
79. Smalheiser, N.R. and N.B. Schwartz, *Cranin: a laminin-binding protein of cell membranes*. *Proceedings of the National Academy of Sciences*, 1987. **84**(18): p. 6457-6461.
80. Smalheiser, N., *Cranin interacts specifically with the sulfatide-binding domain of laminin*. *Journal of neuroscience research*, 1993. **36**(5): p. 528-538.
81. Tomaselli, K., et al., *A neuronal cell line (PC12) expresses two  $\beta 1$ -class integrins— $\alpha 1 \beta 1$ , and  $\alpha 3 \beta 1$ —that recognize different neurite outgrowth-promoting domains in laminin*. *Neuron*, 1990. **5**(5): p. 651-662.

82. Yang, D., et al., *Coordinate control of axon defasciculation and myelination by laminin-2 and-8*. The Journal of cell biology, 2005. **168**(4): p. 655-666.
83. Ruoslahti, E., *Proteoglycans in cell regulation*. J Biol Chem, 1989. **264**(23): p. 13369-13372.
84. Saksela, O., et al., *Endothelial cell-derived heparan sulfate binds basic fibroblast growth factor and protects it from proteolytic degradation*. The Journal of cell biology, 1988. **107**(2): p. 743-751.
85. Rifkin, D.B. and D. Moscatelli, *Recent developments in the cell biology of basic fibroblast growth factor*. The Journal of Cell Biology, 1989. **109**(1): p. 1-6.
86. Ratner, N., et al., *The neuronal cell-surface molecule mitogenic for Schwann cells is a heparin-binding protein*. Proceedings of the National Academy of Sciences, 1988. **85**(18): p. 6992-6996.
87. Yayon, A., et al., *Cell surface, heparin-like molecules are required for binding of basic fibroblast growth factor to its high affinity receptor*. Cell, 1991. **64**(4): p. 841-848.
88. Zhou, F.-Q., et al., *NGF-induced axon growth is mediated by localized inactivation of GSK-3 $\beta$  and functions of the microtubule plus end binding protein APC*. Neuron, 2004. **42**(6): p. 897-912.
89. Romero, M.I., et al., *Functional regeneration of chronically injured sensory afferents into adult spinal cord after neurotrophin gene therapy*. The Journal of Neuroscience, 2001. **21**(21): p. 8408-8416.
90. Lentz, S.I., et al., *Neurotrophins support the development of diverse sensory axon morphologies*. The Journal of neuroscience, 1999. **19**(3): p. 1038-1048.

91. Liu, R.-Y., et al., *NGF enhances sensory axon growth induced by laminin but not by the L1 cell adhesion molecule*. *Molecular and Cellular Neuroscience*, 2002. **20**(1): p. 2-12.
92. Berkemeier, L.R., et al., *Neurotrophin-5: a novel neurotrophic factor that activates trk and trkB*. *Neuron*, 1991. **7**(5): p. 857-866.
93. Squinto, S.P., et al., *trkB encodes a functional receptor for brain-derived neurotrophic factor and neurotrophin-3 but not nerve growth factor*. *Cell*, 1991. **65**(5): p. 885-893.
94. Grothe, C., K. Haastert, and J. Jungnickel, *Physiological function and putative therapeutic impact of the FGF-2 system in peripheral nerve regeneration—lessons from in vivo studies in mice and rats*. *Brain research reviews*, 2006. **51**(2): p. 293-299.
95. Morgan, L., K.R. Jessen, and R. Mirsky, *Negative regulation of the P0 gene in Schwann cells: suppression of P0 mRNA and protein induction in cultured Schwann cells by FGF2 and TGF beta 1, TGF beta 2 and TGF beta 3*. *Development*, 1994. **120**(6): p. 1399-1409.
96. Sendtner, M., et al., *Endogenous ciliary neurotrophic factor is a lesion factor for axotomized motoneurons in adult mice*. *The Journal of neuroscience*, 1997. **17**(18): p. 6999-7006.
97. Kelleher, M., et al., *The use of ciliary neurotrophic factor to promote recovery after peripheral nerve injury by delivering it at the site of the cell body*. *Acta neurochirurgica*, 2006. **148**(1): p. 55-61.
98. McCallister, W.V., et al., *Regeneration along intact nerves using nerve growth factor and ciliary neurotrophic factor*. *Journal of reconstructive microsurgery*, 2004. **20**(6): p. 473-481.

99. Rogister, B., et al., *Transforming growth factor  $\beta$  as a neuronogial signal during peripheral nervous system response to injury*. Journal of neuroscience research, 1993. **34**(1): p. 32-43.
100. Sulaiman, O.A. and T. Gordon, *Transforming growth factor- $\beta$  and forskolin attenuate the adverse effects of long-term Schwann cell denervation on peripheral nerve regeneration in vivo*. Glia, 2002. **37**(3): p. 206-218.
101. Laurencin, C.T. and Y. Khan, *Regenerative engineering*. Science translational medicine, 2012. **4**(160): p. 160ed9-160ed9.
102. James, R., et al., *Electrospun nanofibrous scaffolds for engineering soft connective tissues*. Biomedical nanotechnology: methods and protocols, 2011: p. 243-258.
103. Deister, C., S. Aljabari, and C.E. Schmidt, *Effects of collagen 1, fibronectin, laminin and hyaluronic acid concentration in multi-component gels on neurite extension*. Journal of Biomaterials Science, Polymer Edition, 2007. **18**(8): p. 983-997.
104. Langer, R. and D.A. Tirrell, *Designing materials for biology and medicine*. Nature, 2004. **428**(6982): p. 487-492.
105. Schmalenberg, K.E. and K.E. Uhrich, *Micropatterned polymer substrates control alignment of proliferating Schwann cells to direct neuronal regeneration*. Biomaterials, 2005. **26**(12): p. 1423-1430.
106. Kim, S.-M., S.-K. Lee, and J.-H. Lee, *Peripheral nerve regeneration using a three dimensionally cultured Schwann cell conduit*. Journal of Craniofacial Surgery, 2007. **18**(3): p. 475-488.
107. Pashuck, E.T., H. Cui, and S.I. Stupp, *Tuning supramolecular rigidity of peptide fibers through molecular structure*. Journal of the American Chemical Society, 2010. **132**(17): p. 6041-6046.

108. Cui, H., M.J. Webber, and S.I. Stupp, *Self-assembly of peptide amphiphiles: From molecules to nanostructures to biomaterials*. Peptide Science, 2010. **94**(1): p. 1-18.
109. Hartgerink, J.D., E. Beniash, and S.I. Stupp, *Self-assembly and mineralization of peptide-amphiphile nanofibers*. Science, 2001. **294**(5547): p. 1684-1688.
110. Schense, J.C., et al., *Enzymatic incorporation of bioactive peptides into fibrin matrices enhances neurite extension*. Nature biotechnology, 2000. **18**(4): p. 415-419.
111. Itoh, S., et al., *Hydroxyapatite-coated tendon chitosan tubes with adsorbed laminin peptides facilitate nerve regeneration in vivo*. Brain research, 2003. **993**(1): p. 111-123.
112. Guler, M.O., et al., *Presentation of RGDS epitopes on self-assembled nanofibers of branched peptide amphiphiles*. Biomacromolecules, 2006. **7**(6): p. 1855-1863.
113. Sephel, G., et al., *Laminin A chain synthetic peptide which supports neurite outgrowth*. Biochemical and biophysical research communications, 1989. **162**(2): p. 821-829.
114. Sur, S., et al., *A hybrid nanofiber matrix to control the survival and maturation of brain neurons*. Biomaterials, 2012. **33**(2): p. 545-555.
115. Adams, D.N., et al., *Growth cones turn and migrate up an immobilized gradient of the laminin IKVAV peptide*. Journal of neurobiology, 2005. **62**(1): p. 134-147.
116. Webber, M.J., et al., *Controlled release of dexamethasone from peptide nanofiber gels to modulate inflammatory response*. Biomaterials, 2012. **33**(28): p. 6823-6832.

117. Bulut, S., et al., *Slow release and delivery of antisense oligonucleotide drug by self-assembled peptide amphiphile nanofibers*. *Biomacromolecules*, 2011. **12**(8): p. 3007-3014.
118. Bond, C.W., et al., *Peptide amphiphile nanofiber delivery of sonic hedgehog protein to reduce smooth muscle apoptosis in the penis after cavernous nerve resection*. *The journal of sexual medicine*, 2011. **8**(1): p. 78-89.
119. Ciardelli, G. and V. Chiono, *Materials for peripheral nerve regeneration*. *Macromolecular bioscience*, 2006. **6**(1): p. 13-26.
120. Daly, W., et al., *A biomaterials approach to peripheral nerve regeneration: bridging the peripheral nerve gap and enhancing functional recovery*. *Journal of the Royal Society Interface*, 2012. **9**(67): p. 202-221.
121. Ribeiro-Resende, V.T., et al., *Strategies for inducing the formation of bands of Büngner in peripheral nerve regeneration*. *Biomaterials*, 2009. **30**(29): p. 5251-5259.
122. Mammadov, B., et al., *Cooperative effect of heparan sulfate and laminin mimetic peptide nanofibers on the promotion of neurite outgrowth*. *Acta biomaterialia*, 2012. **8**(6): p. 2077-2086.
123. Mammadov, R., et al., *Heparin mimetic peptide nanofibers promote angiogenesis*. *Biomacromolecules*, 2011. **12**(10): p. 3508-3519.
124. Velichko, Y.S., S.I. Stupp, and M.O. de la Cruz, *Molecular simulation study of peptide amphiphile self-assembly*. *The journal of physical chemistry B*, 2008. **112**(8): p. 2326-2334.
125. Niece, K.L., et al., *Modification of gelation kinetics in bioactive peptide amphiphiles*. *Biomaterials*, 2008. **29**(34): p. 4501-4509.

126. Giancotti, F.G. and E. Ruoslahti, *Integrin signaling*. Science, 1999. **285**(5430): p. 1028-1033.
127. Zaidel-Bar, R., et al., *Hierarchical assembly of cell-matrix adhesion complexes*. Biochemical Society Transactions, 2004. **32**(3): p. 416-420.
128. Guo, W.-h., et al., *Substrate rigidity regulates the formation and maintenance of tissues*. Biophysical journal, 2006. **90**(6): p. 2213-2220.
129. Pelham, R.J. and Y.-l. Wang, *Cell locomotion and focal adhesions are regulated by substrate flexibility*. Proceedings of the National Academy of Sciences, 1997. **94**(25): p. 13661-13665.
130. Wang, H.-B., M. Dembo, and Y.-L. Wang, *Substrate flexibility regulates growth and apoptosis of normal but not transformed cells*. American Journal of Physiology-Cell Physiology, 2000. **279**(5): p. C1345-C1350.
131. Hadjipanayi, E., V. Mudera, and R. Brown, *Close dependence of fibroblast proliferation on collagen scaffold matrix stiffness*. Journal of tissue engineering and regenerative medicine, 2009. **3**(2): p. 77-84.
132. Engler, A., et al., *Substrate compliance versus ligand density in cell on gel responses*. Biophysical journal, 2004. **86**(1): p. 617-628.
133. Engler, A.J., et al., *Matrix elasticity directs stem cell lineage specification*. Cell, 2006. **126**(4): p. 677-689.
134. Saha, K., et al., *Substrate modulus directs neural stem cell behavior*. Biophysical journal, 2008. **95**(9): p. 4426-4438.
135. Armstrong, S.J., et al., *ECM molecules mediate both Schwann cell proliferation and activation to enhance neurite outgrowth*. Tissue engineering, 2007. **13**(12): p. 2863-2870.

136. Bushnell, B.D., et al., *Early clinical experience with collagen nerve tubes in digital nerve repair*. The Journal of hand surgery, 2008. **33**(7): p. 1081-1087.
137. Varejão, A.S., et al., *Methods for the experimental functional assessment of rat sciatic nerve regeneration*. Neurological research, 2004. **26**(2): p. 186-194.
138. Silva, G.A., et al., *Selective differentiation of neural progenitor cells by high-epitope density nanofibers*. Science, 2004. **303**(5662): p. 1352-1355.
139. Tysseling, V.M., et al., *Self-assembling peptide amphiphile promotes plasticity of serotonergic fibers following spinal cord injury*. Journal of neuroscience research, 2010. **88**(14): p. 3161-3170.
140. Wallquist, W., et al., *Laminin chains in rat and human peripheral nerve: distribution and regulation during development and after axonal injury*. Journal of Comparative Neurology, 2002. **454**(3): p. 284-293.
141. Colognato, H. and M.L. Feltri, *Human diseases reveal novel roles for neural laminins*. Trends in neurosciences, 2005. **28**(9): p. 480-486.
142. Gardiner, N.J., et al.,  *$\alpha 7$  integrin mediates neurite outgrowth of distinct populations of adult sensory neurons*. Molecular and Cellular Neuroscience, 2005. **28**(2): p. 229-240.
143. Nodari, A., et al.,  *$\alpha 6 \beta 4$  integrin and dystroglycan cooperate to stabilize the myelin sheath*. The Journal of Neuroscience, 2008. **28**(26): p. 6714-6719.
144. Mammadov, R., et al., *Growth factor binding on heparin mimetic peptide nanofibers*. Biomacromolecules, 2012. **13**(10): p. 3311-3319.
145. Campana, W.M., *Schwann cells: activated peripheral glia and their role in neuropathic pain*. Brain, behavior, and immunity, 2007. **21**(5): p. 522-527.

146. Gaudet, A.D., P.G. Popovich, and M.S. Ramer, *Wallerian degeneration: gaining perspective on inflammatory events after peripheral nerve injury*. J Neuroinflammation, 2011. **8**(1): p. 110.
147. Blakemore, W., *Remyelination of the superior cerebellar peduncle in the mouse following demyelination induced by feeding cuprizone*. Journal of the neurological sciences, 1973. **20**(1): p. 73-83.
148. Perrot, R., et al., *Axonal neurofilaments control multiple fiber properties but do not influence structure or spacing of nodes of Ranvier*. The Journal of Neuroscience, 2007. **27**(36): p. 9573-9584.
149. Klopfeisch, S., et al., *Negative impact of statins on oligodendrocytes and myelin formation in vitro and in vivo*. The Journal of Neuroscience, 2008. **28**(50): p. 13609-13614.
150. Ehrlich, D. and D. Mills, *Myelogenesis and estimation of the number of axons in the anterior commissure of the chick (Gallus gallus)*. Cell and tissue research, 1985. **239**(3): p. 661-666.
151. Grandis, M., et al., *Early abnormalities in sciatic nerve function and structure in a rat model of Charcot-Marie-Tooth type 1A disease*. Experimental neurology, 2004. **190**(1): p. 213-223.
152. Michailov, G.V., et al., *Axonal neuregulin-1 regulates myelin sheath thickness*. Science, 2004. **304**(5671): p. 700-703.
153. Wallace, V.C., et al., *Focal lysolecithin-induced demyelination of peripheral afferents results in neuropathic pain behavior that is attenuated by cannabinoids*. The Journal of neuroscience, 2003. **23**(8): p. 3221-3233.